

Run-and-Tumble particle in inhomogeneous media in one dimension

Prashant Singh

International Centre for Theoretical Sciences, TIFR, Bengaluru 560089, India

Sanjib Sabhapandit

Raman Research Institute, Bangalore, India

Anupam Kundu

International Centre for Theoretical Sciences, TIFR, Bengaluru 560089, India

E-mail: prashant.singh@icts.res.in

Abstract. We investigate the run and tumble particle (RTP), also known as persistent Brownian motion, in one dimension. A telegraphic noise $\sigma(t)$ drives the particle which changes between ± 1 values with some rates. Denoting the rate of flip from 1 to -1 as R_1 and the converse rate as R_2 , we consider the position and direction dependent rates of the form $R_1(x) = \left(\frac{|x|}{l}\right)^\alpha [\gamma_1 \theta(x) + \gamma_2 \theta(-x)]$ and $R_2(x) = \left(\frac{|x|}{l}\right)^\alpha [\gamma_2 \theta(x) + \gamma_1 \theta(-x)]$ with $\alpha \geq 0$. For $\gamma_1 > \gamma_2$, we find that the particle exhibits a steady-state probability distribution even in an infinite line whose exact form depends on α . For $\alpha = 0$ and 1, we solve the master equations exactly for arbitrary γ_1 and γ_2 at large t . From our explicit expression for time-dependent probability distribution $P(x, t)$ we find that it exponentially relaxes to the steady-state distribution for $\gamma_1 > \gamma_2$. On the other hand, for $\gamma_1 < \gamma_2$, the large t behaviour of $P(x, t)$ is drastically different than $\gamma_1 = \gamma_2$ case where the distribution decays as $t^{-\frac{1}{2}}$. Contrary to the latter, detailed balance is not obeyed by the particle even at large t in the former case. For general α , we argue that the approach to the steady state in $\gamma_1 > \gamma_2$ case is exponential which we numerically demonstrate. On the other hand for $\gamma_1 \leq \gamma_2$, the distribution $P(x, t)$ does not reach a steady state, however possesses certain scaling behaviour. For $\gamma_1 = \gamma_2$ we derive this scaling behaviour as well as the scaling function rigorously whereas for $\gamma_1 < \gamma_2$ we provide heuristic arguments for the scaling behaviour and the corresponding scaling functions. We also study the dynamics in semi-infinite line with an absorbing barrier at the origin. We analytically compute the survival probabilities and first-passage time distributions for $\alpha = 0$ and 1. For general $\alpha \geq 0$, once again we compute the value of survival probability at large t and approach to it. Finally, we consider RTP in a finite interval $[0, M]$ and compute the associated exit probability from that interval for all α . All our analytic results match with the numerical simulation of the same.

1. Introduction

Active matter is a class of non-equilibrium systems that can transduce the supplied energy to a systematic movement through some internal mechanisms [1–6]. The dynamics of these systems does not respect time-reversal symmetry and thus break the detailed balance. A plethora of interesting phenomena like - motility induced phase transition [7–9], flocking [10, 11], clustering [12, 13], non existence of equation of state in terms of pressure [14] etc, has been observed and studied in these systems which arise due to the activity and interaction among the particles. At the level of single particle also, such systems exhibit interesting behaviours like accumulation at the boundaries inside confinement [15–17], non-Boltzmann stationary distribution [18–23], anomalous behaviours [24, 25] which are remarkably different than their passive counterparts. "Run-and-tumble" particle (RTP) and Active Brownian particle (ABP) are two paradigmatic models of the dynamics of active particles which have extensively been studied in the recent few years. A single ABP, free or in harmonic trap, shows rich features like anomalous first passage distributions [25], re-entrant phase transition [26], position distribution [27, 28] and many more. These particles have also been used as models of microscopic constituents in many theoretical studies of active matter or collective behaviour of many active agents [19, 29].

The run-and-tumble mechanism describes the stochastic dynamics of a particle which moves in a straight line for some time t_{run} and undergo tumble, a state of rest, which lasts for another time t_{tum} . The particle then chooses the direction randomly for the next run. For example E. Coli bacteria runs for some time along a straight line and then tumbles to randomly choose a new direction of run [30, 31]. For a bacteria such times scales are of the order of $t_{run} \sim 1$ sec and $t_{tum} \sim 0.1$ sec, respectively [31, 32]. In RTP model, such tumble events often considered to occur instantaneously and after each tumble the direction of motion is changed. The time for which the particle runs is taken from exponential distribution with some rate. In one dimension the particle tumbles between the positive and the negative direction and its equation of motion is given by

$$\frac{dx}{dt} = v\sigma(t), \quad (1)$$

where $x(t)$ is the position of the particle at time t , $v(> 0)$ is it's speed and $\sigma(t)$ represents it's instantaneous direction of motion governed by the telegraphic or dichotomous noise. This noise $\sigma(t)$ switches between ± 1 with rate R and consequently it's values at different times are correlated exponentially as $\langle \sigma(t_1)\sigma(t_2) \rangle = 2Re^{-2R|t_1-t_2|}$ which makes the evolution of the position $x(t)$ non-Markovian. The RTP model is in some sense an amalgamation of ballistic motion and Brownian motion as by tuning the parameters R and v , one can go from a pure ballistic particle ($R \rightarrow 0$) to pure Brownian particle ($R \rightarrow \infty$ and $v \rightarrow \infty$ keeping v^2/R fixed). In the physics literature the telegraphic noise and the RTP process have been studied in various settings starting from persistent Brownian motion, electromagnetic theory, optics, Lorentz gas to polymers [33–41].

The model has gained renewed interest in the recent years due to its applicability in mimicking the movement of E-Coli [30]. Also the exact solvability of this model makes it a quintessential candidate for study of the rich and remarkably different behaviours of the active systems. The model has been extensively studied and a variety of its properties are known. Some examples are - joint distribution of maximum and minimum of the position [34], distributions of first-passage times and exit times from an interval [17, 42–44], behaviour under resetting [45], large deviation forms [46–48], convex hull [49], distributions in harmonic trap and other confining potentials [50, 51], behaviour in inhomogeneous force field [52]. Recently the authors have also investigated the "Generalised" Arcsine laws for this model and found some interesting features in comparison to pure Brownian particle [53]. There has also been reasonable amount of study of the microscopic dynamics of multiple interacting RTPs on continuous as well as lattice space [54–59].

It is imperative to emphasise that the telegraphic noise considered in the above settings is characterised only by the constant rate R . The flip from $+1$ to -1 ($1 \rightarrow -1$) occurs with the same rate as from -1 to $+1$ ($-1 \rightarrow 1$). This consideration, however, is a cliché specially when the particle is exposed to some chemoattractants or chemorepellents. For example it is seen experimentally (and used theoretically) [31, 60–63] that in E-Coli the run-time depends strongly on the concentration of the nutrients and the nutrient-gradient. In [31], the run duration for E-Coli is found to depend on whether the bacteria are moving towards or away from the chemo-attractants although the distribution for the times is still exponential. This observation is suggestive to generalise the telegraphic noise in Eq. (1) whereby the flips from $1 \leftrightarrow -1$ occurs with position dependent rates. In this paper we consider the dynamics of a single RTP particle in one dimension with generalised telegraphic noise which is characterised by position and direction dependent rates $R_1(x)$ and $R_2(x)$ given by

$$\begin{aligned} R_1(x) &= \left(\frac{|x|}{l}\right)^\alpha [\gamma_1 \theta(x) + \gamma_2 \theta(-x)], \\ R_2(x) &= \left(\frac{|x|}{l}\right)^\alpha [\gamma_2 \theta(x) + \gamma_1 \theta(-x)], \end{aligned} \tag{2}$$

where $\alpha \geq 0$, $\theta(x)$ is the Heaviside function and, γ_1 and γ_2 (both positive) are position independent rates (see Fig.(1)). Here l is a length scale over which the rate functions are varying. Similar generalisations of RTP motions have been considered in various settings such as Markovian robots [64], active diffusion [65], response to stochastic input [66], chemotaxis [19, 67, 68], quorum sensing [69, 70] and motion with space dependent speed $v(x)$ [71]. These studies mostly deal with either steady-state behaviours or hydrodynamic descriptions. In this paper, we study the occupation probability, the survival problem and the exit problem, going beyond the steady state properties of non-interacting RTPs with flipping rates depending on both position and orientation. We find that, in addition to being proximal to realistic situations, this model of the dynamics of RTP also exhibits interesting features like the existence of steady-state

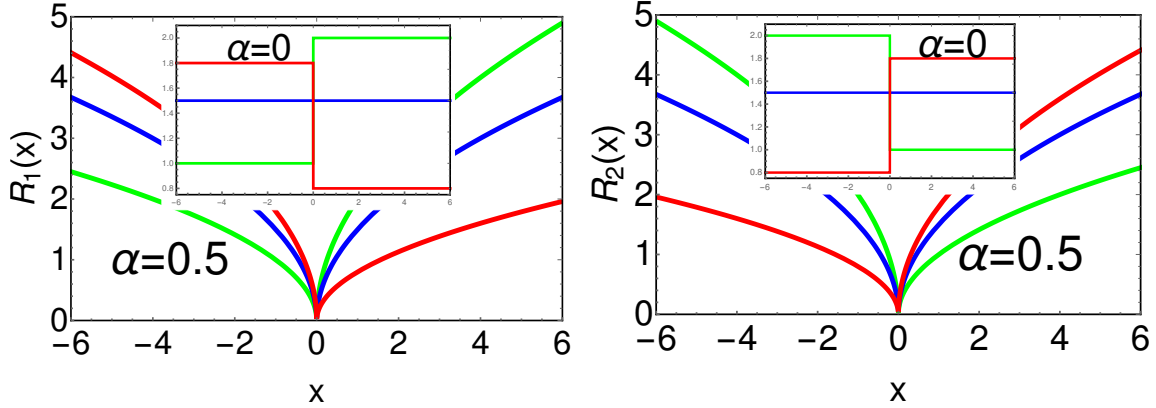


Figure 1. Plot of rates defined in Eqs. (2) for $\alpha = 0.5$ and various signatures of Δ . In the left panel, we have plotted $R_1(x)$ vs x for (i) $\gamma_1 = 2, \gamma_2 = 1$ (green), (ii) $\gamma_1 = \gamma_2 = 1.5$ (blue) and (iii) $\gamma_1 = 0.8, \gamma_2 = 1.8$ (red). **Inset:** Shows the same plot for $\alpha = 0$. In right panel, we have plotted $R_2(x)$ vs x for the same choice of parameters and colour. For all plots $l = 1$.

and non-trivial and richer large time properties of the occupation probability as well as survival probability compared to pure Brownian particles which are otherwise absent in RTPs with constant rate. We find that for this generalised RTP the survival probability $S(t)$ for large time decays as $S(t) \sim t^{-\theta}$ with a persistent exponent θ which strongly depends on α and the rates γ_1 and γ_2 . Note that for a pure Brownian particle as well as for a RTP with constant rate, $\theta = 1/2$.

The paper is organised as follows. We start with the computation of the occupation probability $P(x, t)$ in sec. 2 for different α and $\Delta = (\gamma_1 - \gamma_2)/2$. We perform computations for $\alpha = 0$ in sec. 2.1, for $\alpha = 1$ in sec. 2.2 and for general α in sec. 2.3. For each choices of α , three different cases of $\Delta = 0$, $\Delta > 0$ and $\Delta < 0$ are discussed in subsequent sections. After studying occupation probability $P(x, t)$ we study, survival probability of the RTP in inhomogeneous media with an absorbing site at the origin in sec. 3. In this case also we perform computations for different α separately in secs. 3.1 (for $\alpha = 0$), sec. 3.2 (for $\alpha = 1$) and in sec. 3.3 (for general α). Finally we study exit probability of the RTP from a finite box in sec. 4 which is followed by our conclusion in sec. 5.

2. The occupation probability density

Let $P_\sigma(x, t)$ denote the probability distribution for the RTP, starting at the origin with orientations ± 1 (chosen with probabilities a_\pm such that $a_+ + a_- = 1$), to be at position x in time t with velocity direction $\sigma \in \{+, -\}$. Starting from the Langevin equation (1), it is easy to show that the distributions $P_\pm(x, t)$ satisfy the following master equations [17]

$$\begin{aligned} \partial_t P_+(x, t) &= -v \partial_x P_+(x, t) - R_1(x) P_+(x, t) + R_2(x) P_-(x, t), \\ \partial_t P_-(x, t) &= v \partial_x P_-(x, t) + R_1(x) P_+(x, t) - R_2(x) P_-(x, t), \end{aligned} \quad (3)$$

where $R_1(x)$ and $R_2(x)$ are the position and direction dependent rates defined in Eq. (2). To solve these equations we need to specify the initial as well as the boundary conditions. The initial conditions of the problem are $P_{\pm}(x, 0) = a_{\pm}\delta(x)$. Note that for a given finite time t , the particle can at most travel a distance $\pm vt$ depending on the initial velocity direction which implies the boundary conditions $P_{\pm}(x \rightarrow \pm\infty, t) = 0$. Throughout the paper, we will work with the symmetric initial condition $a_+ = a_- = \frac{1}{2}$ for which the particle starts with $\pm v$ velocity with equal probability. It is interesting to note that the choice of rates $R_1(x)$ and $R_2(x)$ are such that the timescale over which the particle moves towards the origin is $\sim \frac{1}{\gamma_2}$. Similarly, the time scale to go away from the origin is $\frac{1}{\gamma_1}$. For $\gamma_1 > \gamma_2$, the motion is drifted on an average towards the origin which suggests one to anticipate a stationary state distribution at large times even when the particle is moving on an infinite line. On the other hand for $\gamma_1 \leq \gamma_2$, the probability distribution of the particle never reaches a steady state.

To solve the master equations in Eq. (3), we first take Laplace transformation of the distributions with respect to time t , defined as

$$\bar{P}_{\pm}(x, s) = L_{t \rightarrow s}[P_{\pm}(x, t)] = \int_0^{\infty} dt e^{-st} P_{\pm}(x, t), \quad (4)$$

on both sides and get the following ordinary but coupled differential equations for $\bar{P}_{\pm}(x, s)$ as

$$(v\partial_x + R_1(x) + s)\bar{P}_+ = R_2(x)\bar{P}_- + \frac{1}{2}\delta(x), \quad (5)$$

$$(-v\partial_x + R_2(x) + s)\bar{P}_- = R_1(x)\bar{P}_+ + \frac{1}{2}\delta(x). \quad (6)$$

Defining,

$$\bar{P}(x, s) = \bar{P}_+(x, s) + \bar{P}_-(x, s), \quad (7)$$

$$\bar{Q}(x, s) = \bar{P}_+(x, s) - \bar{P}_-(x, s), \quad (8)$$

we rewrite the above equations as

$$v\partial_x \bar{P} + s\bar{Q} + \frac{2 \operatorname{sgn}(x)\Delta |x|^\alpha}{l^\alpha} \bar{P} + \frac{2\gamma |x|^\alpha}{l^\alpha} \bar{Q} = 0, \quad (9)$$

$$s\bar{P} + v\partial_x \bar{Q} = \delta(x), \quad (10)$$

with $2\Delta = \gamma_1 - \gamma_2$ and $2\gamma = \gamma_1 + \gamma_2$. The signum function $\operatorname{sgn}(x)$ takes values 1 for $x > 0$, 0 for $x = 0$ and -1 for $x < 0$. Substituting $\bar{P}(x, s)$ from Eq. (10) in Eq. (9), one can eliminate $\bar{P}(x, s)$ and get a second order differential equation of $\bar{Q}(x, s)$ valid for $x \neq 0$ as,

$$\partial_x^2 \bar{Q} + \frac{2 \operatorname{sgn}(x)\Delta |x|^\alpha}{v l^\alpha} \partial_x \bar{Q} - \left(\frac{2\gamma s |x|^\alpha}{v^2 l^\alpha} + \frac{s^2}{v^2} \right) \bar{Q} = 0. \quad (11)$$

Similarly eliminating $\bar{Q}(x, s)$, one can get the following equation for $\bar{P}(x, s)$

$$s\bar{P}(x, s) - \delta(x) = \partial_x \left(\frac{v^2}{s + \frac{2\gamma |x|^\alpha}{l^\alpha}} \right) \left[\partial_x \bar{P}(x, s) + \frac{2\Delta \operatorname{sgn}(x)|x|^\alpha}{vl^\alpha} \bar{P}(x, s) \right]. \quad (12)$$

To obtain $P(x, t)$ one can in principle directly solve this equation, however, as we will see it turns out convenient to first solve Eq. (11) first and then obtain $\bar{P}(x, s)$ from Eq. (10). To get rid of the first order derivative term (second) in L.H.S of Eq. (11) we define

$$\bar{Q}(x, s) = e^{-\frac{\Delta|x|^{\alpha+1}}{v(\alpha+1)l^\alpha}} G(x, s), \quad (13)$$

substituting which in Eq. (11) and simplifying we get

$$\partial_x^2 G - \left[\frac{\Delta\alpha |x|^{\alpha-1}}{v l^\alpha} + \frac{2\gamma s |x|^\alpha}{v^2 l^\alpha} + \frac{\Delta^2 |x|^{2\alpha}}{v^2 l^{2\alpha}} + \frac{s^2}{v^2} \right] G = 0. \quad (14)$$

We solve this equation with boundary conditions that $G(x, s)$ should not diverge at $x \rightarrow \pm\infty$ for arbitrary α and Δ . This turns out to be difficult job except for $\alpha = 0$ and $\alpha = 1$ for which one can obtain explicit results. For general α , it is however possible to derive some general results. For example, the probability distribution $P_\pm(x, t)$ reaches a stationary state at large times for $\Delta > 0$ with arbitrary $\alpha \geq 0$. For this case ($\gamma_1 > \gamma_2$) particle tumbles from $+1$ to -1 more frequently if it is on the positive side and from -1 to $+1$ more frequently if it is on the negative side. As a result there is an overall effective bias on the particle towards the origin which makes the RTP to reach a stationary state, form of which depends on the value of alpha. On the other hand for $\Delta \leq 0$ the distribution never reaches a stationary state where some properties of the time dependent distribution $P(x, t) = P_+(x, t) + P_-(x, t)$ can be obtained in the asymptotically large time limit. In this limit we demonstrate that the dynamics of the RTP can be described by an effective Langevin equation of a particle diffusing in an inhomogeneous medium with position dependent drift and diffusion constant.

In what follows, we first consider $\alpha = 0$ and $\alpha = 1$ cases separately and consider the general α case in the subsequent section. For each values of α , we discuss the three cases (i) $\Delta > 0$ (ii) $\Delta = 0$ and (iii) $\Delta < 0$ separately.

2.1. Case I: $\alpha = 0$

For this case the rates $R_1(x)$ and $R_2(x)$ are independent of the magnitude of x but depends on the sign of x . In this case, Eq. (14) reduces to

$$\partial_x^2 G - \lambda^2 G = 0, \quad (15)$$

where $\lambda(s) = \frac{1}{v} \sqrt{\Delta^2 + 2\gamma s + s^2}$. We solve this equation with the boundary conditions $G(x \rightarrow \pm\infty, s) = 0$ and using the solution in Eqs. (10) and (13) we finally get $\bar{Q}(x, s)$ and $\bar{P}(x, s)$. For clarity and compactness of the presentation, we have relegated the

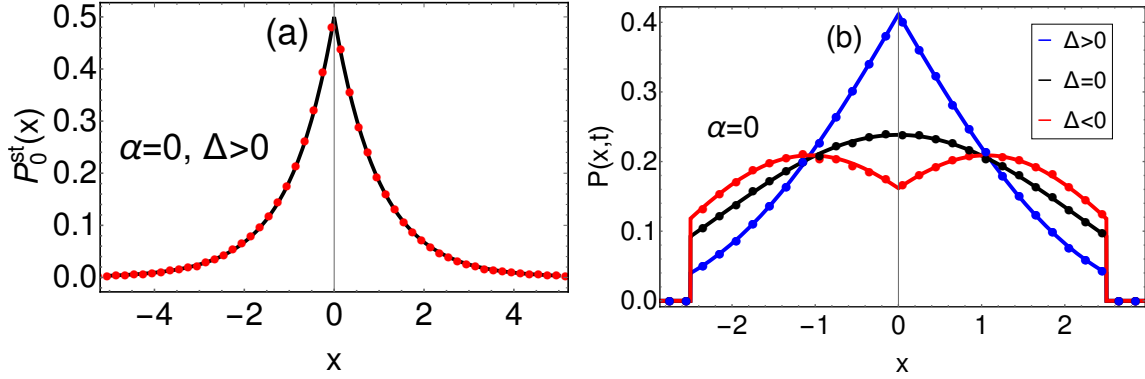


Figure 2. (a) Comparison of the stationary distribution $P_0^{st}(x)$ in Eq.(17) for $\alpha = 0$ with the same obtained from simulation of the microscopic dynamics (shown by filled circles). The parameters chosen are $v = 1, \gamma_1 = 2$ and $\gamma_2 = 1$. The histogram is constructed for 10^6 realisations at time $t = 20$. (b) The time dependent distribution $P(x, t)$ in Eq. (18) of the position of the RTP for $\alpha = 0$ case (solid lines) has been shown in comparison with simulation data (filled circles) for $t = 2.5$. The blue, black and red corresponds to the $\Delta > 0, \Delta = 0$ and $\Delta < 0$. The explicit values for the parametrs for the three curves are given as follows: (i) $\gamma_1 = 1.5, \gamma_2 = 1$ (Blue) (ii) $\gamma_1 = \gamma_2 = 1$ (Black) and (iii) $\gamma_1 = 1, \gamma_2 = 1.5$ (Red). For all plots we have taken $v = 1$.

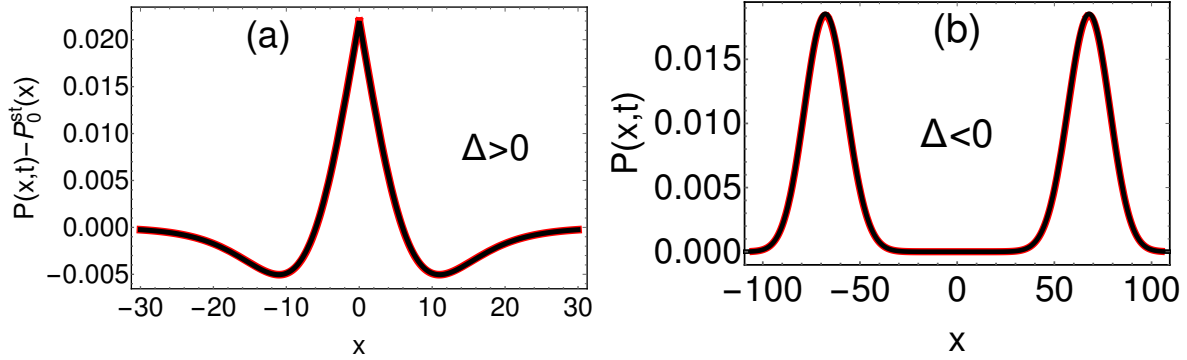


Figure 3. Comparison of the approximate expressions (red) of $P(x, t)$ given in Eq. (19) with the exact result (black) in Eq. (18) for $\Delta \neq 0$. In Figure (a), we have plotted $P(x, t) - P_0^{st}(x)$ vs x for $\gamma_1 = 1.2, \gamma_2 = 1$ and $t = 50$ while in Figure (b), we plot $P(x, t)$ vs x for $\gamma_1 = 1, \gamma_2 = 2$ and $t = 200$. For both plots $v = 1$.

details of calculation of $G(x, s)$ to Appendix A. We here instead present the final expression of $\bar{P}(x, s)$ which reads as

$$\bar{P}(x, s) = \frac{1}{2s} \left(\lambda(s) + \frac{\Delta}{v} \right) e^{-(\lambda(s) + \frac{\Delta}{v})|x|}. \quad (16)$$

Recall that for $\Delta > 0$ (*i.e.* $\gamma_1 > \gamma_2$) one anticipates a stationary state distribution at late times given by

$$P_0^{st}(x) = \lim_{s \rightarrow 0} [s\bar{P}(x, s)] = \frac{\Delta}{v} e^{-\frac{2\Delta}{v}|x|}. \quad (17)$$

which is an exponential distribution decaying over length scale $l_d = \frac{v}{2\Delta}$. In Fig.2(a), we have plotted our analytic result of $P_0^{st}(x)$ in Eq. (17) with the numerical simulation of the same and find excellent agreement. Note that the decay length l_d diverges as $\Delta \rightarrow 0$ which indicates that there is no stationary state for $\Delta = 0$. For $\Delta \leq 0$, the $\lim_{s \rightarrow 0} [s\bar{P}(x, s)] = 0$ again implies that there is no stationary state for this case either.

To get the distribution in time domain, one has to perform the inverse Laplace transform over s (which for Laplace transform $\tilde{f}(s)$ of a function $f(t)$ is denoted by $f(t) = L_{s \rightarrow t}^{-1}[\tilde{f}(s)]$). The details of inversion of $\bar{P}(x, s)$ is relegated to Appendix B and we provide only the final result here.

$$P(x, t) = \frac{1}{2} e^{-\gamma_1 t} \delta(|x| - vt) + \frac{\gamma_1}{2v} \left(1 + \frac{\gamma_2 |x|}{2v} \right) e^{-\frac{\gamma_1 |x|}{2v}} \Theta(vt - |x|) - \frac{\sqrt{\gamma_1 \gamma_2}}{2v} \int_0^t d\tau e^{-\gamma \tau} \frac{d \mathcal{I}(|x|, \tau)}{d|x|} \Theta(v\tau - |x|), \quad (18)$$

where $\mathcal{I}(x, t) = \frac{x e^{-\frac{\Delta x}{v}}}{v} \frac{I_1\left(\sqrt{\gamma_1 \gamma_2 (t^2 - \frac{x^2}{v^2})}\right)}{\sqrt{t^2 - \frac{x^2}{v^2}}}$ with I_1 being the modified Bessel function of first kind. Note that the distribution $P(x, t)$ contains δ -function terms at $x = \pm vt$. They arise from those trajectories in which the particle has not changed its velocity direction till time t starting from $x = 0$ with equal probability for $\pm v$. In Fig.2(b), we plot the above result for $P(x, t)$ for three cases and compare them against the direct simulation of the Langevin equation (1). It is interesting to note that $P(x, t)$ has a dip at $x = 0$ for $\gamma_1 < \gamma_2$ and a peak for $\gamma_1 > \gamma_2$. Appearance of this behaviour can be understood from the fact that for $\gamma_1 < \gamma_2$, the particle is drifted away from the origin while for $\gamma_1 > \gamma_2$ the drift is towards the origin. Another interesting point to note is the derivative of $P(x, t)$ has discontinuity at $x = 0$ for $\gamma_1 \neq \gamma_2$ while it is continuous for $\gamma_1 = \gamma_2$. For $\alpha = 0$ and $\gamma_1 \neq \gamma_2$, the rates $R_1(x)$ and $R_2(x)$ in Eq. (2) have discontinuity at $x = 0$ which amounts to the discontinuity in the derivative of $P(x, t)$. Although the theoretical result in Eq. (18) is exact but less explicit and illuminating. For that it is instructive to get more explicit but approximate expression of the distribution $P(x, t)$ for both $\gamma_1 > \gamma_2$ and $\gamma_1 \leq \gamma_2$ cases in the large time t limit. After some algebra (presented in Appendix C.1 and Appendix C.2 with details) we find the following approximate expressions valid

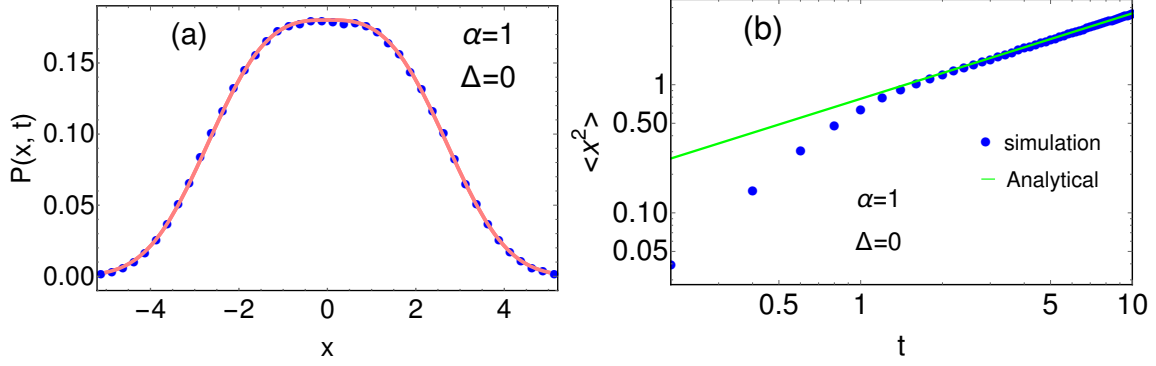


Figure 4. Plots for the case $\alpha = 1$ and $\Delta = 0$. In figure (a) we plot $P(x, t)$ obtained from Eq. (24) (solid line) and compare it with the numerical simulation of Eq. (1) (filled circles) for $t = 10$. In (b), we verify the scaling of $x \sim t^{\frac{1}{3}}$ by plotting $\langle x^2 \rangle$ against t . The Green solid line is the analytic result obtained by using expression for $P(x, t)$ in Eq. (24) while blue filled circles are results of numerical simulation. For both plots, the chosen parameters are $v = 1, \gamma_1 = \gamma_2 = 1.5$ and $l = 1$.

for large t :

$$P(x, t) \simeq \begin{cases} P_0^{st}(x) + \frac{e^{-t[\gamma - \sqrt{\gamma_1 \gamma_2}(1 - \frac{\bar{x}^2}{2}) + \Delta \bar{x}]} \left[\sqrt{\frac{8t\sqrt{\gamma_1 \gamma_2}}{\pi}} |\bar{x}| - te^{t\rho_-^2} \text{Erfc}[\sqrt{t}\rho_-] \left(\Delta \bar{x} + \frac{\rho_+^2 - \rho_-^2}{2} \right) + te^{t\rho_+^2} \text{Erfc}[\sqrt{t}\rho_+] \left(\Delta \bar{x} - \frac{\rho_+^2 - \rho_-^2}{2} \right) \right]}{4|x|}, & \text{if } \gamma_1 > \gamma_2 \\ \frac{1}{\sqrt{4\pi D_0 t}} e^{-\frac{x^2}{4D_0 t}} & \text{if } \gamma_1 = \gamma_2 \\ \sqrt{\frac{\sqrt{\gamma^2 - \Delta^2}}{2\pi t}} \frac{\bar{x}}{2v(1 - \bar{x}^2)^{\frac{3}{4}}} \frac{\bar{x}\sqrt{\gamma^2 - \Delta^2 + \Delta\sqrt{1 - \bar{x}^2}}}{\sqrt{\gamma^2 - \Delta^2 - \gamma\sqrt{1 - \bar{x}^2}}} e^{-t[\Delta \bar{x} + \gamma - \sqrt{\gamma^2 - \Delta^2}\sqrt{1 - \bar{x}^2}]}, & \text{if } \gamma_1 < \gamma_2 \end{cases} \quad (19)$$

with $D_0 = \frac{v^2}{2\gamma}$, $\bar{x} = \frac{|x|}{vt}$ and $\rho_{\pm} = \sqrt{\gamma - \sqrt{\gamma_1 \gamma_2}} \pm \bar{x} \sqrt{\frac{\sqrt{\gamma_1 \gamma_2}}{2}}$. In Figure (3) we have compared these approximate results with the exact result in Eq. (18).

2.2. Case II: $\alpha = 1$

We now focus on the second analytically solvable case $\alpha = 1$ in which the equation (14) becomes

$$\partial_x^2 G - \left[\frac{\Delta}{vl} + \frac{2\gamma s |x|}{v^2 l} + \frac{s^2}{v^2} + \frac{\Delta^2 x^2}{v^2 l^2} \right] G = 0. \quad (20)$$

We first look at the $\Delta = 0$ case.

2.2.1. $\Delta = 0$

For this case Eq. (20) becomes,

$$\partial_x^2 G(x, s) - \left[\frac{2\gamma s |x|}{v^2 l} + \frac{s^2}{v^2} \right] G(x, s) = 0 \quad (21)$$

We identify this equation as Airy differential equation whose general solutions are Airy functions. Satisfying appropriate boundary conditions, one finally gets $G(x, s)$ (see Appendix D.1 for details) using which in Eqs.(10) and (13) provides

$$\bar{P}(x, s) = -\frac{1}{2s} \frac{d}{d|x|} \left[\frac{\text{Ai}\left(c s^{\frac{1}{3}} |x| + d s^{\frac{4}{3}}\right)}{\text{Ai}\left(d s^{\frac{4}{3}}\right)} \right], \quad (22)$$

where $c = \left(\frac{2\gamma}{v^2 l}\right)^{\frac{1}{3}}$, $d = \frac{c l}{2\gamma}$ and $\text{Ai}(x)$ is the Airy function of the first kind. Although it is possible to perform inverse Laplace transform for arbitrary t , it is however more interesting to look at the behaviour at large t , to obtain which one can neglect $O(s^{\frac{4}{3}})$ terms inside the argument of the Airy function in the numerator of Eq. (22). Using $\text{Ai}(z) = \frac{\sqrt{z}}{\sqrt{3\pi}} K_{\frac{1}{3}}\left(\frac{2}{3}z^{\frac{3}{2}}\right)$ we get

$$\bar{P}(x, s) \simeq -\frac{1}{2s} \frac{d}{d|x|} \left[\frac{\text{Ai}\left(c s^{\frac{1}{3}} |x|\right)}{\text{Ai}(0)} \right] = \frac{c^2 |x|}{2\sqrt{3\pi}\text{Ai}(0)s^{\frac{1}{3}}} K_{\frac{2}{3}}\left(\frac{2}{3}(c|x|)^{\frac{3}{2}}\sqrt{s}\right), \quad (23)$$

where $K_{\frac{2}{3}}(y)$ is Modified Bessel function. Performing the inverse Laplace transform we get

$$P(x, t) = \frac{1}{4\pi\text{Ai}(0)t^{\frac{1}{6}}} \sqrt{\frac{3c}{|x|}} e^{-\frac{|x|^3 c^3}{18t}} W_{\frac{1}{6}, \frac{1}{3}}\left(\frac{|x|^3 c^3}{9t}\right), \quad (24)$$

where $W_{m,\nu}(x)$ is the Whittaker function. To arrive at the above result we have used the following result

$$L_{s \rightarrow t}^{-1} [2\sqrt{g} s^{m-1} K_{2\nu}(2\sqrt{gs})] = t^{\frac{1}{2}-m} e^{-\frac{g}{2t}} W_{m-\frac{1}{2}, \nu}\left(\frac{g}{t}\right), \quad (25)$$

for $g > 0$. In Figure 4(a), we compare our result for the distribution $P(x, t)$ in Eq. (24) against numerical simulation where we notice excellent agreement. For very large t , one can simplify the expression for $P(x, t)$ further by using the asymptotic of $W_{\frac{1}{6}, \frac{1}{3}}(z) \approx z^{\frac{1}{6}} e^{-\frac{z}{2}}$ for $z \rightarrow 0$ and $\text{Ai}(0) = \frac{\Gamma(\frac{1}{3})}{2\pi 3^{\frac{1}{6}}}$. We get

$$P(x, t) \simeq \frac{1}{t^{\frac{1}{3}}} f_0\left(\frac{x}{t^{\frac{1}{3}}}\right), \quad \text{where, } f_0(y) = \frac{3^{\frac{1}{3}} c}{2\Gamma(\frac{1}{3})} e^{-\frac{|y|^3 c^3}{9}}. \quad (26)$$

Remember $c = \left(\frac{2\gamma}{v^2 l}\right)^{\frac{1}{3}}$. This result implies that for $\alpha = 1$ with $\Delta = 0$, the position x of the particle scales as $x \sim t^{\frac{1}{3}}$ for large t which is different from the $\alpha = 0$ case for which $x \sim \sqrt{t}$. To numerically verify this, we plot variance $\langle x^2 \rangle$ against t in Figure 4(b) and at large t we indeed observe the scaling behaviour $\langle x^2 \rangle \sim t^{\frac{2}{3}}$. We will later see that the above scaling behaviour gets generalised for general $\alpha > 0$.

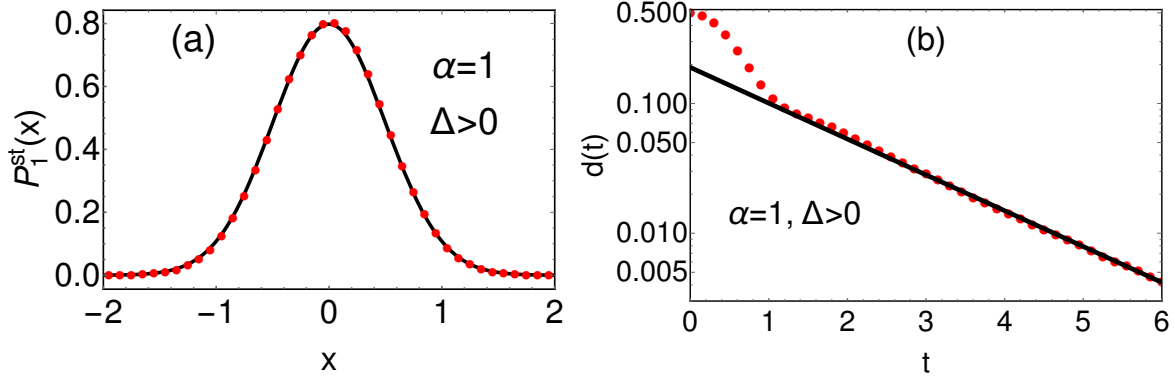


Figure 5. (a) Comparison of the stationary distribution $P_1^{st}(x)$ in Eq.(28) for $\alpha = 1$ (solid line) with simulation of the Langevin equation (shown by filled circles). The parameters chosen are $v = 1, l = 0.5, \gamma_1 = 3$ and $\gamma_2 = 1$. The histogram is constructed for 10^6 realisations at time $t = 30$. (b) Here we plot $d(t) = \text{var}(\infty) - \text{var}(t)$ where the variance is $\text{var}(t) = \langle x(t)^2 \rangle - \langle x(t) \rangle^2$. The simulation result (shown by filled circles) is plotted with $d(t) \sim e^{-\zeta t}$ (shown by thick line) with $\zeta = 0.636$ is given by solution of Eq. (29) with largest real part. The parameters chosen are $\gamma_1 = 3.5, \gamma_2 = 1.5, v = 1$ and $l = 1$.

2.2.2. $\Delta \neq 0$

Here we consider the $\Delta \neq 0$ case for $\alpha = 1$, for which we solve Eq. (20). Note that the general solutions of this equation can be expressed in terms of parabolic cylinder functions $D_{\mu-1/2}(x)$. Choosing the integration constants appropriately to satisfy the boundary conditions, one obtains $G(x, s)$, using which in Eqs.(10) and (13) we get (see Appendix D.2 for details)

$$\bar{P}(x, s) = -\frac{1}{2s} \frac{d}{d|x|} \left[\frac{e^{-\frac{\Delta}{2vl}x^2} D_{\beta s^2 - \frac{1+\text{sgn}(\Delta)}{2}} \left(\sqrt{\frac{2|\Delta|}{vl}} \left(|x| + \frac{\gamma sl}{\Delta^2} \right) \right)}{D_{\beta s^2 - \frac{1+\text{sgn}(\Delta)}{2}} \left(\sqrt{\frac{2|\Delta|}{vl}} \frac{\gamma sl}{\Delta^2} \right)} \right], \quad (27)$$

where $\beta = \frac{l(\gamma^2 - \Delta^2)}{2v|\Delta|^3}$. Note that for $\Delta > 0$, we have $\mu(s) = \nu s^2$. Just like the $\alpha = 0$ case, in this case also we anticipate stationary state for $\Delta > 0$ which can be determined from the limit $\lim_{s \rightarrow 0} [s\bar{P}(x, s)]$. Using $D_{-1}(z) = \sqrt{\frac{\pi}{2}} e^{\frac{z^2}{4}} \text{Erfc}(\frac{z}{\sqrt{2}})$, we get

$$P_1^{st}(x) = \sqrt{\frac{\gamma_1 - \gamma_2}{2\pi vl}} e^{-\frac{\gamma_1 - \gamma_2}{2vl}x^2}, \quad (28)$$

for $\Delta > 0$ where the subscript 1 in $P_1^{st}(x)$ stands for $\alpha = 1$. In Figure 5(a), we have plotted $P_1^{st}(x)$ and compared it with the direct numerical simulation of the microscopic equation (1). We find excellent agreement between the two. To understand the relaxation to this stationary state one needs to take into account the contribution from the pole with second largest real part (largest pole is $s = 0$ which gives the steady state) in the Laplace inversion procedure. The poles of $\bar{P}(x, s)$ in Eq. (27), come from the

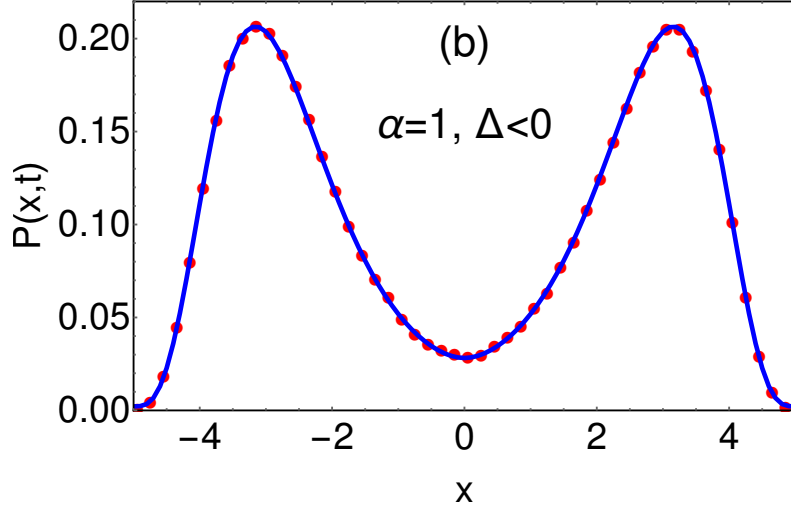


Figure 6. Comparison of the probability distribution $P(x,t)$ for $\alpha = 1$ and $\Delta < 0$ with the numerical simulation. The theoretical curve (solid line) is obtained by performing inverse Laplace transform in Eq. (30). For this plot the parameters we have taken are $\gamma_1 = 1$, $\gamma_2 = 3$, $v = 1$, $l = 1$ and $t = 5$.

zeros of $D_{\beta s^2-1} \left(\sqrt{\frac{2|\Delta|}{vl} \frac{\gamma sl}{\Delta^2}} \right)$ which lie on the negative real axis. The pole ζ with largest real part other than 0 will set the time scale $|\zeta|^{-1}$ for the exponential relaxation which can be determined by solving

$$D_{\beta \zeta^2-1} \left(\sqrt{\frac{2|\Delta|}{vl} \frac{\gamma \zeta l}{\Delta^2}} \right) = 0, \quad (29)$$

numerically for $\Delta > 0$. To verify this result we compute $d(t) = \text{var}(\infty) - \text{var}(t)$ where $\text{var}(t) = \langle x^2 \rangle - \langle x \rangle^2$ is the variance obtained from the numerical simulation, which should decay to zero as $\sim e^{-\zeta t}$. In Figure 5(b) we plot $d(t)$ as a function of t and indeed observe the exponential decay with time scale $|\zeta|^{-1}$.

For $\Delta < 0$, as we have argued earlier there is no stationary state. In this case, the solution $\bar{P}(x,s)$ in the Laplace space, given in Eq. (27), becomes

$$\bar{P}(x,s) = -\frac{1}{2s} \frac{d}{d|x|} \left[e^{-\frac{\Delta}{2vl} x^2} \frac{D_{\beta s^2} \left(\sqrt{\frac{2|\Delta|}{vl} (|x| + \frac{\gamma sl}{\Delta^2})} \right)}{D_{\beta s^2} \left(\sqrt{\frac{2|\Delta|}{vl} \frac{\gamma sl}{\Delta^2}} \right)} \right], \quad (30)$$

where $\beta = \frac{l(\gamma^2 - \Delta^2)}{2v|\Delta|^3}$. Performing the inverse Laplace transform, we can obtain $P(x,t)$. For the parameters $\gamma_1 = 1$, $\gamma_2 = 3$, $v = 1$, $l = 1$ and $t = 5$ we perform the inverse Laplace transform numerically to get $P(x,t)$ at $t = 5$ which we compare with simulation results in Fig. 6 and observe excellent agreement. The convergence of the numerical inversion procedure becomes poor with increasing t . However, following a different approximate procedure, explained in the next section, we find that for large t ,

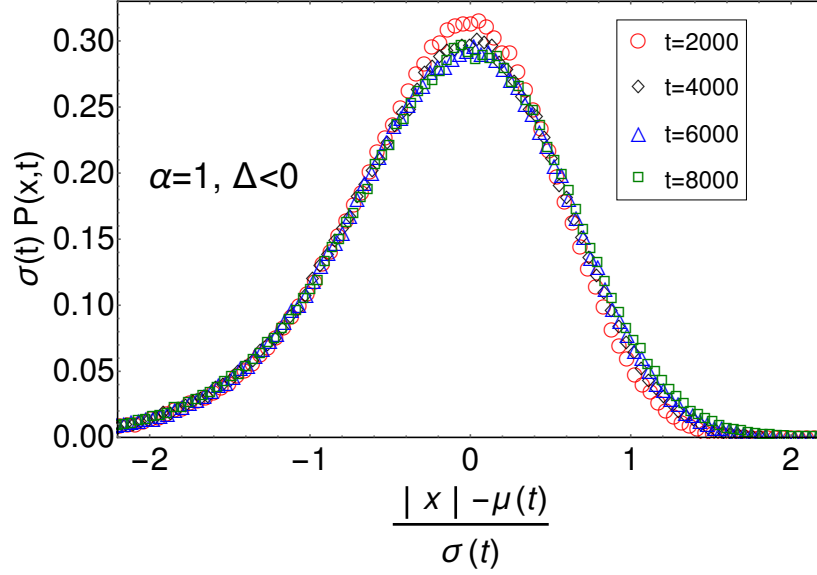


Figure 7. Verification of the scaling behaviour of the distribution $P(x, t) = \frac{1}{2\sigma_1(t)} \mathcal{G}_1\left(\frac{|x| - \mu(t)}{\sigma_1(t)}\right)$ for $\alpha = 1$ where $\mu(t) = \langle |x| \rangle$ and $\sigma_1^2(t) = \langle x^2 \rangle - \langle |x| \rangle^2$. Here we have shown the scaling behaviour only for positive x as the distribution $P(x, t)$ is symmetric. Other parameters of the plot are $\gamma_1 = 1.5$, $\gamma_2 = 1.6$, $v = 1$ and $l = 1$.

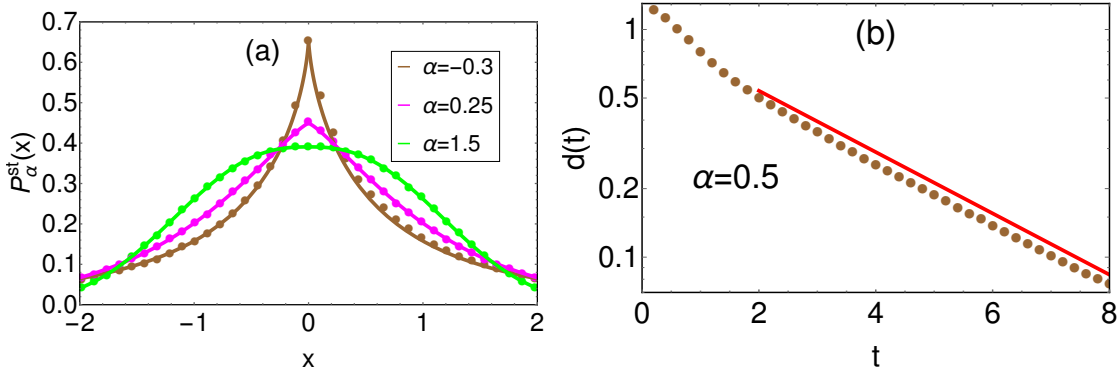


Figure 8. (a) Comparison of the stationary state distribution $P_\alpha^{st}(x)$ obtained in Eq. (33) (solid lines) with the numerical simulation data (filled circles) for three values of α . The histogram has been constructed using 10^6 realisations at $t = 15$. (b) Numerical simulation of $d(t)$ defined as $d(t) = \text{var}(\infty) - \text{var}(t)$ where $\text{var}(t) = \langle x(t)^2 \rangle - \langle x(t) \rangle^2$. We find $d(t) \sim e^{-\zeta t}$ (shown by red line) where we numerically find $\zeta = 0.31$. For both plots, we have taken $\gamma_1 = 2$, $\gamma_2 = 1$, $l = 1$ and $v = 1$.

the distribution $P(x, t)$ has the following scaling form $P(x, t) \simeq \frac{1}{2\sigma_1(t)} \mathcal{G}\left(\frac{|x| - \mu(t)}{\sigma_1(t)}\right)$ with $\mu(t) = \langle |x| \rangle = \frac{v|\Delta|}{\gamma} t$ and $\sigma_1^2(t) = \langle x^2 \rangle - \langle |x| \rangle^2 = (vl/|\Delta|) \ln(t)$. In Fig. 7 we verify this scaling behaviour numerically. In the next section we show that $\mathcal{G}(u)$ is a mean zero and unit variance Gaussian.

2.3. Case III: General α

We now look at the general $\alpha (> 0)$ case. For this case making concrete analytical progress from Eq. (20) for any Δ is difficult. However, it is possible to obtain some results for the occupation probability distribution in asymptotically large times. To proceed, in this case, it seems convenient to start from the original master equations in (3) which, by defining $P(x, t) = P_+(x, t) + P_-(x, t)$ and $Q(x, t) = P_+(x, t) - P_-(x, t)$, can be rewritten, in terms of $R_{\pm}(x) = \frac{R_1(x) \pm R_2(x)}{2}$, as

$$\partial_t P(x, t) = -v \partial_x Q(x, t), \quad (31)$$

$$\partial_t Q(x, t) = -R_+(x)Q(x, t) - R_-(x)P(x, t) - v \partial_x P(x, t). \quad (32)$$

2.3.1. $\Delta > 0$: We first present the $\Delta > 0$ case for reasons that will be self-evident later. In this case the particle reaches a stationary state, to obtain which we equate the time derivative on the left hand side of Eqs. (31) and (32) to zero and then solve for the x dependence. We get the following expression for the stationary state distribution

$$P_{\alpha}^{st}(x) = \frac{1}{2 \Gamma\left(1 + \frac{1}{\alpha+1}\right)} \left[\frac{(\gamma_1 - \gamma_2)}{v l^{\alpha} (\alpha + 1)} \right]^{\frac{1}{\alpha+1}} e^{-\frac{(\gamma_1 - \gamma_2)}{v(\alpha+1)l^{\alpha}} |x|^{\alpha+1}}. \quad (33)$$

Note that for $\alpha = 0$ and $\alpha = 1$, this expression correctly reduces to the exponential and Gaussian distributions given in Eqs. (17) and (28) respectively. In Fig. 8a we numerically verify the above form of the steady state distribution $P_{\alpha}^{st}(x)$ for three choices of α different from $\alpha = 0$ and 1. Approach to this steady state can in principle be understood by looking at the time dependent solutions of Eqs. (31) and (32) at large times, however finding such solutions is a difficult task for which one has to solve the eigenvalue equation (14). Note that this eigenvalue equation looks similar to Schroedinger equation but it is actually different from it. In the $\alpha = 0$ and $\alpha = 1$ case we have seen that for $\Delta > 0$ the approach to steady state is exponential. For general $\alpha \geq 0$ also we expect exponential relaxation with a time scale determined from the structure of effective potential. In Fig. 8b, we indeed observe that the relaxation is exponential where we plot the convergence of the $\text{var}(t) = \langle x(t)^2 \rangle$ to its value at $t \rightarrow \infty$.

2.3.2. $\Delta \leq 0$: As seen in the previous two exactly solvable cases $\alpha = 0$ and $\alpha = 1$, for general $\alpha \geq 0$ also we expect that the distribution $P(x, t)$ for general α also does not reach a stationary state for $\Delta \leq 0$. To proceed, we first note in Eqs. (31) and (32) that the equation for $P(x, t)$ is in the form of a continuity equation. On the other hand the equation for $Q(x, t)$ is not in this form, but has decay terms proportional to the rates $R_{\pm}(x)$ which are non-negative functions. As a result, at large times the difference distribution $Q(x, t)$ would not depend on time explicitly. Only time dependence would come from $P(x, t)$. Neglecting $\partial_t Q(x, t)$ for large t , we get $R_+(x)Q(x, t) = -R_-(x)P(x, t) - v \partial_x P(x, t)$, inserting which in Eq. (31) we get

$$\partial_t P(x, t) = \frac{v^2 l^{\alpha}}{2\gamma} \partial_x (|x|^{-\alpha} \partial_x P(x, t)) + \text{sgn}(x) \frac{v\Delta}{\gamma} \partial_x P(x, t). \quad (34)$$

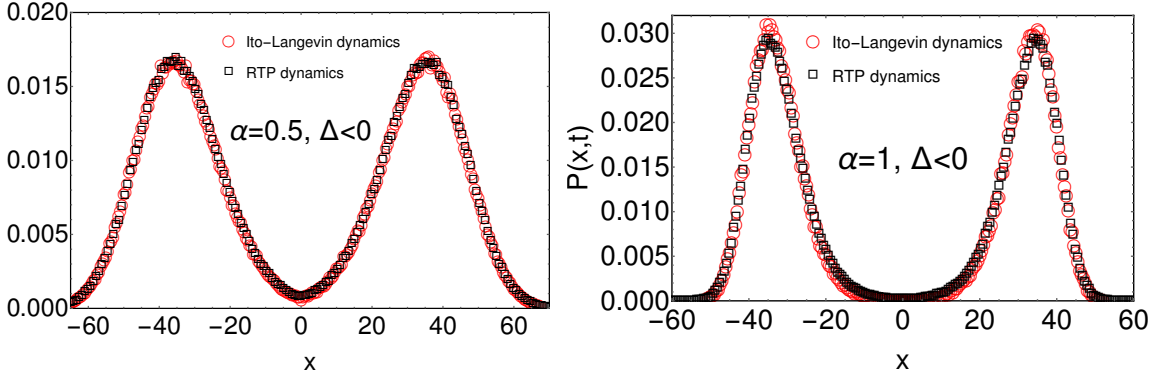


Figure 9. Comparison of the probability distribution obtained from simulation of the effective Langevin equation (36) (red circles) with the same from the original RTP dynamics (1) (black squares) for $\alpha = 0.5$ and $\alpha = 1.0$. For both values of α the histograms are obtained at $t = 1000$ with $\gamma_1 = 1.5$ and $\gamma_2 = 1.6$. Other common parameters are $v = 1$ and $l = 1$.

This equation can also be derived from Eq. (12). Performing inverse Laplace transform over the s variable on both sides of this equation, we get

$$\partial_t P(x, t) = \partial_x \int_0^t dt' e^{-2\gamma \frac{|x|^\alpha}{l^\alpha} (t-t')} \left[v^2 \partial_x P(x, t') + \frac{2v\Delta \operatorname{sgn}(x) |x|^\alpha}{l^\alpha} P(x, t) \right]. \quad (35)$$

For large $|x|$, the exponential term in the above equation can be approximated by $\sim \frac{l^\alpha}{2\gamma |x|^\alpha} \delta(t - t')$ and as a result the above equation reduces to Eq. (34). Note that this approximation does not work for $\alpha = 0$. It works only for $\alpha > 0$. The equation (34) can be interpreted as the Fokker-Planck equation of a particle diffusing in an inhomogeneous environment of diffusion constant $\mathcal{D}(x) = \frac{v^2 l^\alpha}{\gamma |x|^\alpha}$ and drift $\mathcal{V}(x) = -\operatorname{sgn}(x) \left[\frac{v\Delta}{\gamma} + \frac{\alpha v^2 l^\alpha}{2\gamma |x|^{\alpha+1}} \right]$. The corresponding Ito-Langevin equation is given by

$$\frac{dx}{dt} = \mathcal{V}(x) + \sqrt{\mathcal{D}(x)} \eta(t), \quad (36)$$

where $\eta(t)$ is the Gaussian white noise with $\langle \eta(t) \rangle = 0$ and $\langle \eta(t) \eta(t') \rangle = \delta(t - t')$. Comparison between the two dynamics is shown in Fig. 9 where we have plotted $P(x, t)$ *vs.* x obtained from the simulation of the effective Langevin equation (36) and the same from the original RTP dynamics (1) at $t = 1000$ for two values of $\alpha = 0.5$ (Fig. 9b) and $\alpha = 1.0$ (Fig. 9a).

$\Delta = 0$: For this the second term on the right hand side of Eq. (34) is absent. It is easy to check that the solution of this equation, for large t , is given by [72]

$$P(x, t) \simeq \frac{1}{t^{\frac{1}{2+\alpha}}} f_\alpha \left(\frac{|x|}{t^{\frac{1}{2+\alpha}}} \right), \quad \text{with } f_\alpha(z) = \frac{(2+\alpha)^{\frac{\alpha}{2+\alpha}}}{2\Gamma\left(\frac{1}{2+\alpha}\right) D_\alpha^{\frac{1}{2+\alpha}}} e^{-\frac{z^{2+\alpha}}{(2+\alpha)^2 D_\alpha}}, \quad (37)$$

where $D_\alpha = \frac{v^2 l^\alpha}{2\gamma}$. Note that for $\alpha = 1$ the scaling function $f_\alpha(z)$ correctly reduces to the scaling function in Eq. (26). The function $f_\alpha(z)$ is plotted in Fig. 10 for two different

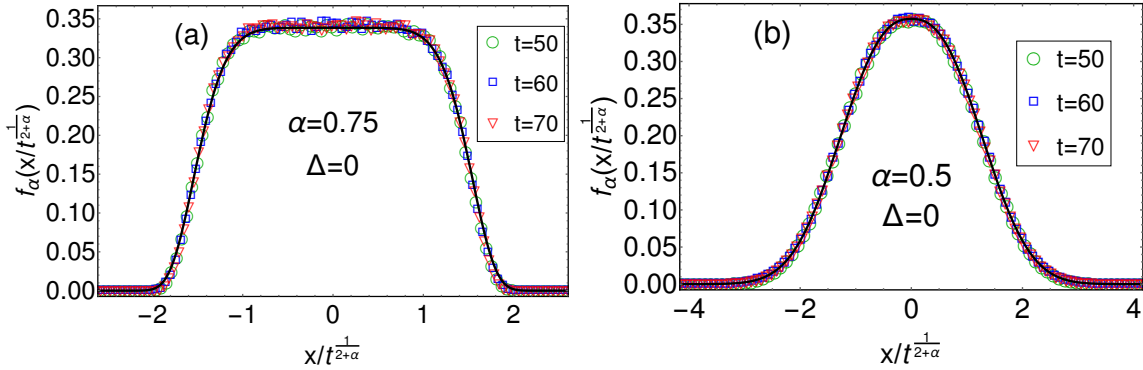


Figure 10. (a) Scaling function $f_\alpha(z)$ in Eq. (37) is plotted (solid black line) and compared with the results (symbols) obtained by simulating the RTP equation (1) at three different times $t = 50, 60, 70$ for $\alpha = 0.75$ (a) and $\alpha = 0.5$ (b) with $\gamma_1 = \gamma_2 = 1.5$. Other common parameters are $v = 1$ and $l = 1$

values of α and compared with the numerical simulation for three different times. We observe excellent agreement between the theory and the simulation results.

$\Delta < 0$: For this case the drift $\mathcal{V}(x)$ on the particle, as can be seen from Eq. (34), is away from the origin on both sides at large x . As a result the particle never reach a steady state as also has been argued earlier. We already have observed numerically in Fig. 9 that at large times the dynamics of the RTP can be well described by the Langevin equation (36). From this comparison, we also observe that the distribution $P(x, t)$ is symmetric with respect to the origin which implies that the mean position of the particle is zero, however the average value of the absolute position $\mu(t) = \langle |x| \rangle$ is not zero. The two symmetric peaks one the opposite sides of the origin are situated at $x = \pm\mu(t)$. For large t , this quantity increases linearly as $\langle |x| \rangle = \mu(t) \sim \frac{v|\Delta|}{\gamma}t$, which can be easily verified numerically. In particular, it can be shown that, using the following variable transforms $|x| = \mu(t) + z$ and $\tau = t^{1-\alpha}$ the Eq. (34) in the large t limit becomes the following diffusion equation

$$\partial_\tau P(z, \tau) = \mathcal{D}_\alpha \partial_z^2 P(z, \tau), \quad (38)$$

where $\mathcal{D}_\alpha = \frac{v^2 \ell^\alpha}{\gamma(1-\alpha)} \left(\frac{\gamma}{v|\Delta|} \right)^\alpha$ for $0 < \alpha < 1$. This immediately implies that for large t , the distribution $P(x, t)$ has the following scaling form

$$P(x, t) \simeq \frac{1}{2\sigma_\alpha(t)} \mathcal{G} \left(\frac{|x| - \mu(t)}{\sigma_\alpha(t)} \right) \quad (39)$$

where $\mathcal{G}(u)$ satisfies the differential equation $\partial_u^2 \mathcal{G}(u) + u \partial_u \mathcal{G}(u) + \mathcal{G}(u) = 0$ and the variance $\sigma_\alpha^2(t) = \langle x^2 \rangle - \langle |x| \rangle^2$ is given by $\sigma_\alpha^2(t) \sim \mathcal{D}_\alpha t^{1-\alpha}$. The solution of this equations is very simple and given by the zero mean and unit variance Gaussian, $\mathcal{G}(u) = e^{-u^2/2}/\sqrt{2\pi}$. The same procedure can also be followed for $\alpha = 1$ and one gets same scaling behaviour (as in Eq. (39)) with same scaling function $\mathcal{G}(u)$ but not

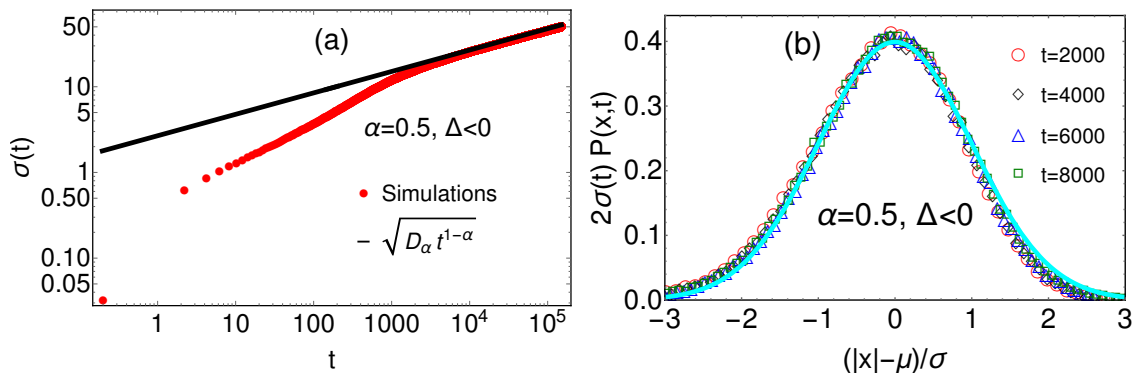


Figure 11. (a) Numerical verification of $\sigma^2(t) \sim \mathcal{D}_\alpha t^{1-\alpha}$ with $\mathcal{D}_\alpha = \frac{v^2 \ell^\alpha}{\gamma(1-\alpha)} \left(\frac{\gamma}{v|\Delta|} \right)^\alpha$ for large t . (b) Numerical verification of the scaling behaviour in Eq. (39) with $\mathcal{G}_\alpha(u)$ given by $\mathcal{G}_\alpha(u) = e^{-u^2/2}/\sqrt{2\pi}$ (shown by solid line). For both plots, we have taken $\alpha = 0.5, \gamma_1 = 1.5, \gamma_2 = 1.6, l = 1$ and $v = 1$.

$\sigma_1^2(t) \sim (vl/|\Delta|) \ln(t)$ for $\alpha = 1$. The time dependence of the variance $\sigma_\alpha^2(t)$ is verified numerically in Fig. 11a for $\alpha < 1$. In the numerical simulation of the equation of motion (1) with the rates given in Eqs. (2) we have chosen $\alpha = 0.5$. It turns out that this value is optimal for the numerical verification. For given γ and Δ , the description given by the FP equation (34) starts becoming valid at (large) times which increases with decreasing α . Performing numerical simulation over such huge time duration turns out to be highly expensive. On the other hand, for larger α , even though the effective inhomogeneous diffusion equation (34) starts becoming valid at time earlier than smaller alpha, but the rates (being $\propto |x|^\alpha$) also increases faster with time because for $\Delta < 0$ the particles is effectively drifted away from the origin. As a result, one requires a very small dt in the numerical simulation in order to get good convergence, which in turn again makes the computation expensive.

The scaling behavior in Eq. (39) is demonstrated and verified in Fig. 11b numerically again for $\alpha = 0.5$. Note that this scaling behaviour is valid for $0 < \alpha < 1$. For $\alpha > 1$, we numerically observe that the variance decreases with time. As a result at very large time we expect the distribution $P(x, t)$ to shrink to a sum of two delta functions at $x = \pm\mu(t)$ which one would naively guess when a similar procedure as done for $0 < \alpha \leq 1$ is attempted for $\alpha > 1$ case.

3. Survival probability

In this section we study the motion of the RTP with space dependent rates in Eq. (2) in presence of an absorbing barrier. In many physical settings, how long does a particle survive from a given absorbing site is of primary interest [75]. In particular, we will consider the absorbing site to be at the origin and address the question of survival probability for the particle starting from some position $x_0 > 0$. Let $S_\pm(x_0, t)$ denote the survival probability for the RTP with initial position x_0 and initial velocity $\pm v$ in presence of an absorbing wall at $x = 0$. We start by deriving the backward master

equations satisfied by $S_{\pm}(x_0, t)$ and then solve them explicitly. Below we briefly discuss the derivation of the backward master equations.

The probability that RTP with initial velocity direction $+$ survives from the absorbing wall at $x = 0$ till time $t + dt$ is $S_+(x_0, t + dt)$. One can break the total time duration $t + dt$ into two parts (i) $[0, dt]$ and (ii) $[dt, t + dt]$. In the first interval of duration dt , the RTP can do two things: (a) without flipping its direction move to position $x_0 + vdt$ with probability $(1 - R_1(x_0)dt)$ and, (b) flip its direction of motion with probability $R_1(x_0)dt$. After time dt , the RTP survives the remaining interval with probability $S_+(x_0 + vdt, t)$, if event (a) occurs and with probability $S_-(x_0, t)$ if event (b) occurs. Adding all these probabilities with appropriate weights one gets $S_+(x_0, t + dt) = (1 - R_1(x_0)dt)S_+(x_0 + vdt, t) + R_1(x_0)dt S_-(x_0, t)$. Similarly, if the initial velocity direction is negative, then one has $S_-(x_0, t + dt) = (1 - R_2(x_0)dt)S_-(x_0 - vdt, t) + R_2(x_0)dt S_+(x_0 + vdt, t)$. Performing Taylor series expansion in dt and taking $dt \rightarrow 0$ limit, one gets the following backward master equations for $S_{\pm}(x_0, t)$

$$\begin{aligned}\partial_t S_+(x_0, t) &= v\partial_{x_0} S_+(x_0, t) - R_1(x_0)S_+(x_0, t) + R_1(x_0)S_-(x_0, t), \\ \partial_t S_-(x_0, t) &= -v\partial_{x_0} S_-(x_0, t) + R_2(x_0)S_+(x_0, t) - R_2(x_0)S_-(x_0, t).\end{aligned}\quad (40)$$

To solve these equations, one needs to specify the initial condition as well as the boundary conditions. Note that if the particle starts from $x_0 \rightarrow \infty$ initially, then for all finite t it survives regardless of its initial velocity direction. This gives rise $S_{\pm}(x_0 \rightarrow \infty, t) = 1$. To understand the other boundary condition $S_-(0, t) = 0$, the particle will be instantly absorbed if it starts at $x_0 = 0$ with $-$ velocity. However if the particle starts from $x_0 = 0$ with $+$ velocity, it will not get absorbed instantly and accordingly one gets $S_+(0, t) \neq 0$. Hence for any $x_0 \neq 0$ we have $S_{\pm}(x_0, 0) = 1$.

To solve Eqs. (40) we take Laplace transformation with respect to t as $\bar{S}_{\pm}(x_0, s) = \int_0^{\infty} dt e^{-st} S_{\pm}(x_0, t)$ to get

$$\begin{aligned}[-v\partial_{x_0} + R_1(x_0) + s] \bar{S}_+(x_0, s) &= 1 + R_1(x_0)\bar{S}_-(x_0, s), \\ [v\partial_{x_0} + R_2(x_0) + s] \bar{S}_-(x_0, s) &= 1 + R_2(x_0)\bar{S}_+(x_0, s),\end{aligned}\quad (41)$$

where we have used the the initial conditions $S_{\pm}(x_0, 0) = 1$, Eqs. (40). Under this transformation the boundary conditions become $\bar{S}_{\pm}(x_0 \rightarrow \infty, s) = \frac{1}{s}$ and $\bar{S}_-(0, s) = 0$. Note that the differential equations in Eqs. (41) are inhomogeneous. To make them homogeneous we define $\bar{U}_{\pm}(x_0, s)$ such that

$$\bar{S}_{\pm}(x_0, s) = \frac{1}{s} + \bar{U}_{\pm}(x_0, s), \quad (42)$$

which also simplifies the boundary conditions as $\bar{U}_{\pm}(x_0 \rightarrow \infty, s) = 0$. The Eqs. (41) now become

$$\begin{aligned}[-v\partial_{x_0} + R_1(x_0) + s] \bar{U}_+ &= R_1(x_0)\bar{U}_-, \\ [v\partial_{x_0} + R_2(x_0) + s] \bar{U}_- &= R_2(x_0)\bar{U}_+.\end{aligned}\quad (43)$$

Further defining,

$$\begin{aligned}\bar{U}(x_0, s) &= \bar{U}_+(x_0, s) + \bar{U}_-(x_0, s), \\ \bar{H}(x_0, s) &= \bar{U}_+(x_0, s) - \bar{U}_-(x_0, s),\end{aligned}\quad (44)$$

we get

$$\partial_{x_0}^2 \bar{H} - \frac{2\Delta x_0^\alpha}{v l^\alpha} \partial_{x_0} \bar{H} - \left[\frac{2\Delta \alpha x_0^{\alpha-1}}{v l^\alpha} + \frac{2\gamma s x_0^\alpha}{v^2 l^\alpha} + \frac{s^2}{v^2} \right] \bar{H} = 0, \quad (45)$$

$$\text{and,} \quad \bar{U}(x_0, s) = \frac{v}{s} \partial_{x_0} \bar{H} - \frac{2\Delta x_0^\alpha}{s l^\alpha} \bar{H}. \quad (46)$$

One can get rid of first order derivative in Eq. (45) by making the transformation,

$$\bar{H}(x_0, s) = e^{\frac{\Delta}{v(\alpha+1)l^\alpha} x_0^{\alpha+1}} F(x_0, s), \quad (47)$$

using which in Eq. (45), one gets

$$\partial_{x_0}^2 F(x_0, s) - \left[\frac{\Delta \alpha x_0^{\alpha-1}}{v l^\alpha} + \frac{2\gamma s x_0^\alpha}{v^2 l^\alpha} + \frac{\Delta^2 x_0^{2\alpha}}{v^2 l^{2\alpha}} + \frac{s^2}{v^2} \right] F(x_0, s) = 0. \quad (48)$$

Note that this equation is identical to Eq. (14) for $G(x, s)$ obtained in the previous section except for the boundary conditions which are different for the two cases. In what follows, we will solve this equation for $\alpha = 0$ and $\alpha = 1$ separately and then address the case of general α .

3.1. Case I: $\alpha = 0$

We start with the simplest case of $\alpha = 0$. For this case the rates $R_{1,2}(x)$ are actually x independent. Recall that x_0 is the initial position of the RTP which is greater than 0. Hence noting that $F(x_0, s)$ is finite as $x_0 \rightarrow \infty$, one gets $F(x_0, s) \sim e^{-\lambda(s)x_0}$ where $\lambda(s) = \frac{1}{v} \sqrt{2\gamma s + s^2 + \Delta^2}$ (see Appendix A for details). Inserting this in Eqs. (46) and (47) and finally writing for $\bar{S}_\pm(x_0, s)$, the expressions read as,

$$\bar{S}_\pm(x_0, s) = \frac{1}{s} + \frac{\mathcal{A}}{2s} e^{\left(\frac{\Delta}{v} - \lambda(s)\right)x_0} [-\Delta - v\lambda(s) \pm s], \quad (49)$$

where \mathcal{A} is a constant independent of x_0 . To evaluate \mathcal{A} , we use the boundary condition $\bar{S}_-(0, s) = 0$ which gives $\mathcal{A}(s) = \frac{2}{\Delta + s + v\lambda(s)}$. Finally inserting this in Eq. (49) we get the following the expressions for $\bar{S}_\pm(x_0, s)$

$$\bar{S}_-(x_0, s) = \frac{1}{s} - \frac{1}{s} e^{\left(\frac{\Delta}{v} - \lambda(s)\right)x_0}, \quad (50)$$

$$\bar{S}_+(x_0, s) = \frac{1}{s} - \frac{s + \gamma - v\lambda(s)}{s\gamma_2} e^{\left(\frac{\Delta}{v} - \lambda(s)\right)x_0}. \quad (51)$$

Using the following results for inverse Laplace transformations,

$$\begin{aligned}
L_{s \rightarrow t} [e^{-\lambda(s)x_0}] &= -ve^{\frac{\Delta x_0}{v}} \frac{d}{dx_0} \left[e^{-\gamma t} I_0 \left(\sqrt{\gamma_1 \gamma_2 \left(t^2 - \frac{x_0^2}{v^2} \right)} \right) \Theta(vt - x_0) \right], \\
L_{s \rightarrow t} [(s + \gamma - v\lambda(s))e^{-\lambda(s)x_0}] &= \sqrt{\gamma_1 \gamma_2} \frac{e^{-\gamma t + \frac{\Delta x_0}{v}}}{t + \frac{x_0}{v}} \left[\frac{x_0 \sqrt{\gamma_1 \gamma_2}}{v} I_0 \left(\sqrt{\gamma_1 \gamma_2 \left(t^2 - \frac{x_0^2}{v^2} \right)} \right) \right. \\
&\quad \left. + \sqrt{\frac{vt - x_0}{vt + x_0}} I_1 \left(\sqrt{\gamma_1 \gamma_2 \left(t^2 - \frac{x_0^2}{v^2} \right)} \right) \right] \Theta(vt - x_0) \tag{52}
\end{aligned}$$

we get

$$\begin{aligned}
S_-(x_0, t) &= 1 + ve^{\frac{\Delta x_0}{v}} \frac{d}{dx_0} \int_0^t d\tau e^{-\gamma \tau} I_0 \left(\sqrt{\gamma_1 \gamma_2 \left(\tau^2 - \frac{x_0^2}{v^2} \right)} \right) \Theta(v\tau - x_0), \\
S_+(x_0, t) &= 1 - \sqrt{\frac{\gamma_1}{\gamma_2}} e^{\frac{\Delta x_0}{v}} \int_0^t d\tau \frac{e^{-\gamma \tau}}{\tau + \frac{x_0}{v}} \Theta(v\tau - x_0) \left[\frac{x_0 \sqrt{\gamma_1 \gamma_2}}{v} I_0 \left(\sqrt{\gamma_1 \gamma_2 \left(\tau^2 - \frac{x_0^2}{v^2} \right)} \right) \right. \\
&\quad \left. + \sqrt{\frac{v\tau - x_0}{v\tau + x_0}} I_1 \left(\sqrt{\gamma_1 \gamma_2 \left(\tau^2 - \frac{x_0^2}{v^2} \right)} \right) \right] \tag{53}
\end{aligned}$$

For $\gamma_1 = \gamma_2$ the above expressions match with the previously obtained results in [17, 53]. In figure 12 we have plotted our above theoretical results for $S_{\pm}(x_0, t)$ and compared with the numerical simulations. We observe excellent agreement between them. Notice that for both $S_{\pm}(x_0, t)$ remain 1 till time $t_b = \frac{x_0}{v}$. This is because the RTP initially starting from x_0 will take at least time t_b to reach the absorbing wall at $x = 0$. Before t_b , the RTPs do not feel presence of the barrier. Once they reach the wall with velocity $-v$ at time t_b^- , a fraction of them will change the velocity from $-$ to $+$ and survive the wall, while others will get absorbed at time t_b+ . This results in sudden drop in the population of RTPs as indicated by the sudden drop in $S_-(x_0, t)$. However no sudden drop occurs in $S_+(x_0, t)$ because the particles do not reach the wall with $+$ velocity.

It is worth noting that the particle is drifted away from the origin for $\Delta < 0$ which gives rise to non-zero $S_{\pm}(x_0, t)$ as $t \rightarrow \infty$. This can be, in principle, verified by putting $t \rightarrow \infty$ in the expressions of $S_{\pm}(x_0, t)$ given in Eqs. (53). However it turns out more convenient to obtain this from the Laplace transforms given in Eqs. (50) and (51) by putting $s = 0$ which corresponds to $t \rightarrow \infty$ limit. Hence for $\Delta < 0$ we get, $\mathcal{S}_{\pm}(x_0) = S_{\pm}(x_0, t \rightarrow \infty) = \lim_{s \rightarrow 0} [s\bar{S}_{\pm}(x_0, s)]$ given by

$$\begin{aligned}
\mathcal{S}_+(x_0) &= 1 - \frac{\gamma - |\Delta|}{\gamma + |\Delta|} e^{-\frac{2|\Delta|}{v}x_0}, \\
\mathcal{S}_-(x_0) &= 1 - e^{-\frac{2|\Delta|}{v}x_0}. \tag{54}
\end{aligned}$$

One can similarly compute $\mathcal{S}_{\pm}(x_0)$ for $\Delta \geq 0$ which turns out to be 0 as the particle will definitely reach origin after a sufficient time interval.

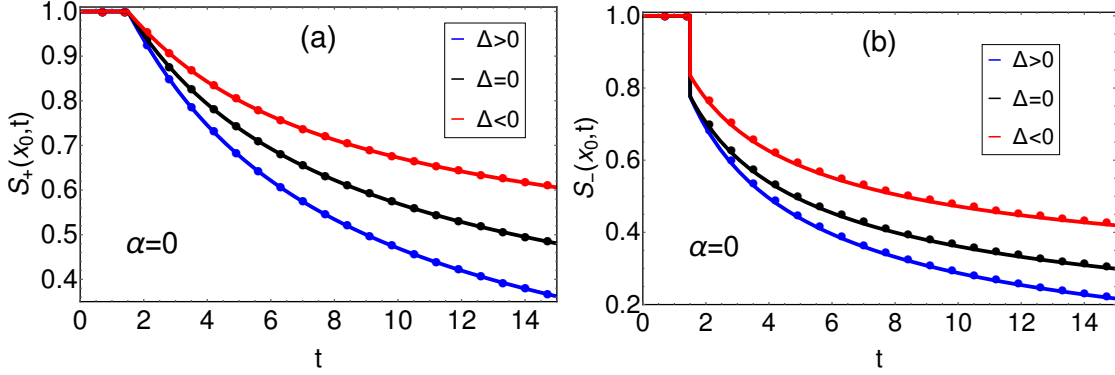


Figure 12. Comparison of $S_{\pm}(x_0, t)$ given by Eqs. (53) for $\alpha = 0$ with the simulation results (filled circles) for various signatures of Δ . In both (a) and (b), we have chosen (i) $\gamma_1 = 1.2$ $\gamma_2 = 1$ for blue, (ii) $\gamma_1 = \gamma_2 = 1$ for black and (iii) $\gamma_1 = 1$ $\gamma_2 = 1.2$ for red. Other parameters chosen are $x_0 = 1.5$, $v = 1$ and $l = 1$.

We now discuss the behaviour of $S_{\pm}(x_0, t)$ for large t which would provide the relaxation to this stationary value for $\Delta \geq 0$. For this, we take the large t approximation in Eqs. (53). The detail of this calculation is given in Appendix E and we present only the final results here. Defining $L_{\pm}(x_0, t) = S_{\pm}(x_0, t) - \mathcal{S}_{\pm}(x_0)$, where $\mathcal{S}_{\pm}(x_0)$ is 0 for $\Delta \geq 0$ and given by Eqs. (54) for $\Delta < 0$, we obtain

$$L_+(x_0, t) \approx \begin{cases} \sqrt{\frac{\gamma_1}{\gamma_2}} \left(\frac{x_0}{v} + \frac{1}{\sqrt{\gamma_1 \gamma_2}} \right) \frac{(\gamma_1 \gamma_2)^{\frac{1}{4}} e^{\frac{\Delta x_0}{v}}}{\sqrt{2\pi t^3} (\gamma - \sqrt{\gamma_1 \gamma_2})} e^{-t(\gamma - \sqrt{\gamma_1 \gamma_2})}, & \text{if } \gamma_1 \neq \gamma_2 \\ \frac{1}{\sqrt{\pi t}} \frac{\sqrt{2\gamma}}{v} \left(x_0 + \frac{v}{\gamma} \right), & \text{if } \gamma_1 = \gamma_2. \end{cases} \quad (55)$$

$$L_-(x_0, t) \approx \begin{cases} \frac{x_0}{v} \frac{(\gamma_1 \gamma_2)^{\frac{1}{4}} e^{\frac{\Delta x_0}{v}}}{\sqrt{2\pi t^3} (\gamma - \sqrt{\gamma_1 \gamma_2})} e^{-t(\gamma - \sqrt{\gamma_1 \gamma_2})}, & \text{if } \gamma_1 \neq \gamma_2 \\ \frac{1}{\sqrt{\pi t}} \frac{x_0 \sqrt{2\gamma}}{v}, & \text{if } \gamma_1 = \gamma_2. \end{cases} \quad (56)$$

Our results for $\Delta = 0$ match with that in [17, 58]. Note that for $\Delta > 0$, the survival probabilities decay exponentially whereas for $\Delta = 0$ case it decays as a power law $\sim 1/\sqrt{t}$. In fact the time scale $\tau_r = \frac{1}{\gamma - \sqrt{\gamma_1 \gamma_2}}$ associated to this exponential decay diverges in the $\Delta \rightarrow 0$ ($\gamma_1 \rightarrow \gamma_2$) limit which is consistent with the power law behaviour for $\Delta = 0$. For $\Delta < 0$ case, we observe that S_{\pm} relaxes exponentially to their stationary values over the same time scale $\tau_r = \frac{2\gamma}{\Delta^2}$. The divergence of τ_r as $\Delta \rightarrow 0$ implies that the stationary survival probabilities do not exist for $\Delta = 0$ case. From the expressions, we see that for $x_0 = 0$ while S_- is exactly 0, S_+ still has a non-zero value. The particle can survive if it starts from origin with positive velocity. In Figure (13) we have compared these asymptotic behaviours with the exact results in Eqs. (53).

3.2. Case II: $\alpha = 1$

We now turn to the $\alpha = 1$ case. For this case the rates $R_{1,2}(x)$ of the orientation flipping decays as $\sim |x|^{-1}$ which, as we will see, makes the large time behaviour for the survival

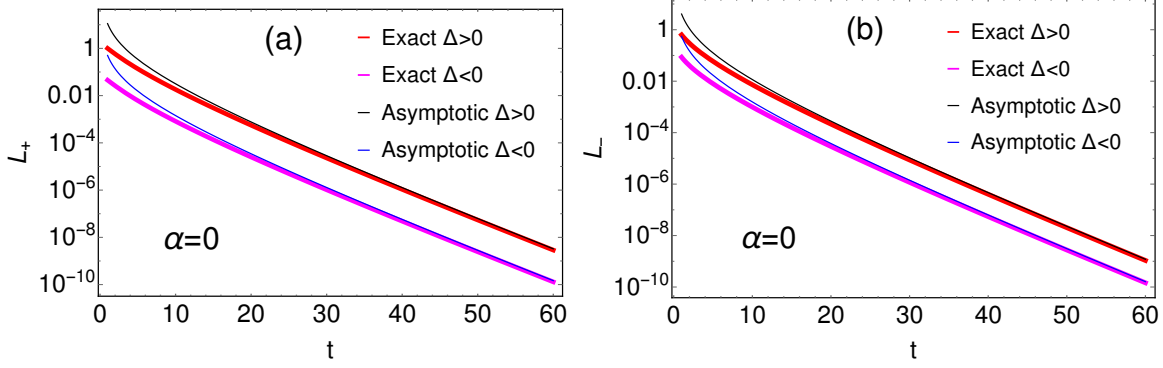


Figure 13. Comparison of the asymptotic behaviour of $S_{\pm}(x_0, t)$ given by Eqs. (55) and (56) with the exact expression in Eq. (53) for $\alpha = 0$ and for both $\Delta > 0$ and $\Delta < 0$. We have plotted $L_{\pm}(x_0, t) = S_{\pm}(x_0, t) - S_{\pm}(x_0, t \rightarrow \infty)$. In both (a) and (b) we have chosen (i) $\gamma_1 = 3, \gamma_2 = 1$ for red and (ii) $\gamma_1 = 1, \gamma_2 = 3$ for magenta. Other common parameters are $v = 1$ and $x_0 = 1$.

probability different from the $\alpha = 0$ case. This difference is most prominent in the $\Delta = 0$ case which we consider next. In the subsequent sections we discuss the $\Delta \neq 0$ cases.

3.2.1. $\Delta = 0$

We start with Eq. (48) which for $\alpha = 1$ and $\Delta = 0$ takes the form

$$\partial_{x_0} F(x_0, s) - \left(\frac{2\gamma s x_0}{v^2 l} + \frac{s^2}{v^2} \right) F(x_0, s) = 0 \quad (57)$$

Since the general solutions of this equation are same to Eq. (21) we take the solutions from Appendix D and write a general solution for $F(x_0, s)$ in terms of Airy functions and the integration constants C_{\pm} . Inserting the $F(x_0, s)$ in Eq. (47) and then in Eq. (46), and fixing the integration constants through the boundary conditions, we finally get

$$\bar{S}_{\pm}(x_0, s) = \frac{1}{s} - \frac{1}{s} \frac{v c \text{Ai}'\left(cx_0 s^{\frac{1}{3}} + ds^{\frac{4}{3}}\right) \pm s^{\frac{2}{3}} \text{Ai}\left(cx_0 s^{\frac{1}{3}} + ds^{\frac{4}{3}}\right)}{v c \text{Ai}'(0) - s^{\frac{2}{3}} \text{Ai}(0)} \quad (58)$$

with $c = \left(\frac{2\gamma}{v^2 l}\right)^{\frac{1}{3}}$ and $d = \frac{c l}{2\gamma}$ where in the end we have used the definitions in Eqs. (44). Performing inverse Laplace transform for arbitrary s is hard and also not so illuminating. We focus on the large t behaviour, to get which we neglect the $ds^{4/3}$ term in the argument of the Airy function and get the following simpler equation

$$\bar{S}_{\pm}(x_0, s) \simeq \frac{1}{s} - \frac{1}{s v c |\text{Ai}'(0)|} \left[v c \text{Ai}'(cx_0 s^{\frac{1}{3}}) \pm s^{\frac{2}{3}} \text{Ai}(cx_0 s^{\frac{1}{3}}) - \frac{s^{\frac{2}{3}} \text{Ai}(0)}{|\text{Ai}'(0)|} \text{Ai}'(cx_0 s^{\frac{1}{3}}) \right] \quad (59)$$

Now once again using $\text{Ai}(z) = \frac{\sqrt{z}}{\sqrt{3\pi}} K_{\frac{1}{3}}\left(\frac{2}{3}z^{\frac{3}{2}}\right)$ and using Eq. (25) we perform the inverse

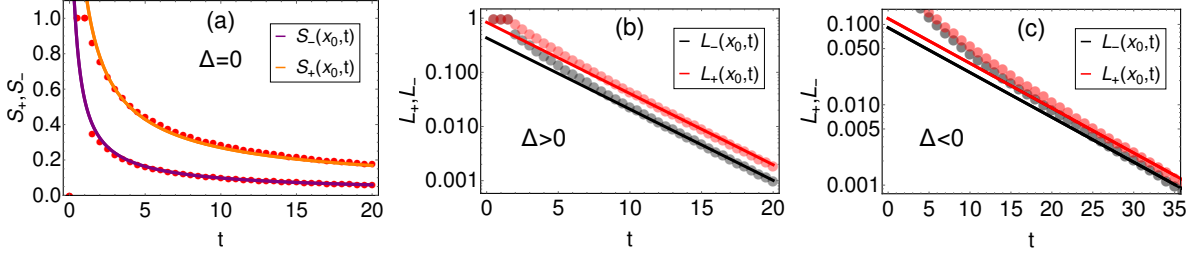


Figure 14. Comparison of the analytic results of $S_{\pm}(x_0, t)$ with the numerical simulation for $\alpha = 1$ and $\Delta = 0$ (a), $\Delta > 0$ (b) and $\Delta < 0$ (c). In Figure (a), we have plotted Eq. (60) for $\gamma_1 = \gamma_2 = 1$ and $x_0 = 1$. For Figures (b) and (c), we define $L_{\pm}(x_0, t) = S_{\pm}(x_0, t) - \mathcal{S}_{\pm}(x_0)$ with $\mathcal{S}_{\pm}(x_0)$ equal to 0 for $\Delta > 0$ and given by Eqs. (65) for $\Delta < 0$. The analytic expressions for $L_{\pm}(x_0, t)$, given by Eqs. (66) for both $\Delta < 0$ and $\Delta > 0$, are plotted (solid line) and compared with the simulation data (filled circles). For Figure (b), we have taken $x_0 = 1.5, \gamma_1 = 2$ and $\gamma_2 = 1$ while for Figure (c), we have taken $x_0 = 1.5, \gamma_1 = 1$ and $\gamma_2 = 1.5$. For all three figures, other common parameters are $v = 1$ and $l = 1$.

of the Laplace transform to get

$$S_{\pm}(x_0, t) \simeq 1 + \frac{e^{-\frac{x_0^3 c^3}{18t}}}{2\pi\sqrt{3}gvc |Ai'(0)|} \left[\frac{cx_0 Ai(0)}{|Ai'(0)|\sqrt{t}} W_{\frac{1}{2}, \frac{1}{3}} \left(\frac{x_0^3 c^3}{9t} \right) - vc^2 x_0 t^{\frac{1}{6}} W_{-\frac{1}{6}, \frac{1}{3}} \left(\frac{x_0^3 c^3}{9t} \right) \right] \pm \frac{\sqrt{cx_0}}{t^{\frac{1}{3}}} W_{\frac{1}{3}, \frac{1}{6}} \left(\frac{x_0^3 c^3}{9t} \right). \quad (60)$$

In Figure 14(a), we have plotted our result of $S_{\pm}(x_0, t)$ alongwith with the results from numerical simulations where we observe perfect match at large t . The mismatch at smaller t is self-explanatory. Although the expression in Eq. (60) is nice but still less illuminating. It is more instructive to find the large t asymptotic of $S_{\pm}(x_0, t)$. For this, we use the following representation of the Whittaker function $W_{k,m}(z) = e^{-\frac{z}{2}} z^{m+\frac{1}{2}} U(\frac{1}{2}+m-k, 1+2m, z)$, where $\mathcal{U}(a, b, z)$ is the confluent hypergeometric function of second kind which, for $z \rightarrow 0$ behaves as $\mathcal{U}(a, b, z) \approx \frac{\Gamma(b-1)}{\Gamma(a)} z^{1-b} + \frac{\Gamma(1-b)}{\Gamma(a-b+1)}$ with $\Gamma(a)$ being the Gamma function. Using this asymptotic form in Eq. (60) we get

$$S_+(x_0, t) \approx \frac{1}{2\pi 3^{\frac{5}{6}} t^{\frac{2}{3}}} \left(-x_0^2 c^2 \Gamma \left(-\frac{2}{3} \right) + \frac{6\Gamma(\frac{1}{3})}{vc} \right),$$

$$S_-(x_0, t) \approx -\frac{1}{2\pi 3^{\frac{5}{6}} t^{\frac{2}{3}}} x_0^2 c^2 \Gamma \left(-\frac{2}{3} \right) \quad (61)$$

suggesting a power law decay with persistent exponent $\theta = 2/3$. Note that this exponent is different from the exponent $\theta = 1/2$ in the $\alpha = 0$ case (see Eqs (55) and (56)). Another interesting feature to note is while $S_-(x_0, t)$ vanishes if $x_0 = 0$, $S_+(x_0, t)$ still has a non-zero value (which decays with t) as we have seen in the $\alpha = 0$ case.

3.2.2. $\Delta \neq 0$

We now consider $\Delta \neq 0$ case for which the Eq. (48) reduces to

$$\partial_{x_0}^2 F - \left[\frac{\Delta}{vl} + \frac{2\gamma s x_0}{v^2 l} + \frac{s^2}{v^2} + \frac{\Delta^2 x_0^2}{v^2 l^2} \right] F = 0. \quad (62)$$

We note that this equation is identical to Eq. (20) although the boundary conditions of the two equations are different. However, the general solutions of the two equations are same and can be expressed in terms of the parabolic cylinder functions $D_\mu(y)$ as shown in Appendix D. Inserting this general solution in Eqs. (46) and (47) and using the boundary conditions $\bar{S}_-(x_0 \rightarrow 0, s) = 0$ we, after performing some simplifications, get

$$\bar{S}_\pm(x_0, s) = \frac{1}{s} - \frac{1}{s} e^{\frac{\Delta x_0^2}{2vl}} \frac{\mathcal{N}_\pm(x_0, s)}{\mathcal{N}_-(0, s)}, \quad (63)$$

where

$$\begin{aligned} \mathcal{N}_\pm(x_0, s) = & \sqrt{\frac{2v|\Delta|}{l}} \{ \beta s^2 \Theta(-\Delta) + \Theta(\Delta) \} D_{\beta s^2 - \Theta(-\Delta)} \left(\sqrt{\frac{2|\Delta|}{vl}} \left(x_0 + \frac{\gamma sl}{\Delta^2} \right) \right) \\ & - s \frac{\gamma \pm \Delta}{|\Delta|} D_{\beta s^2 - \Theta(\Delta)} \left(\sqrt{\frac{2|\Delta|}{vl}} \left(x_0 + \frac{\gamma sl}{\Delta^2} \right) \right), \end{aligned} \quad (64)$$

with $\beta = \frac{l(\gamma^2 - \Delta^2)}{2v|\Delta|^3}$ and $\Theta(x)$ is the Heaviside theta function. To get the survival probabilities in the time domain one needs to perform inverse Laplace transform. As we are interested in the behaviour at large t , we look at behaviour of $\bar{S}_\pm(x_0, s)$ for small s . In particular, the $\lim_{s \rightarrow 0} [s\bar{S}_\pm]$ gives the survival probability as $t \rightarrow \infty$. For $\Delta < 0$ using $D_0(z) = e^{-\frac{z^2}{4}}$, we get

$$\begin{aligned} \mathcal{S}_+(x_0) &= 1 - \frac{\gamma - |\Delta|}{\gamma + |\Delta|} e^{-\frac{|\Delta|x_0^2}{vl}}, \\ \mathcal{S}_-(x_0) &= 1 - e^{-\frac{|\Delta|x_0^2}{vl}}. \end{aligned} \quad (65)$$

where $\mathcal{S}_\pm(x_0) = S_\pm(x_0, t \rightarrow \infty)$. Similarly one can compute $\lim_{s \rightarrow 0} [s\bar{S}_\pm]$ for $\Delta > 0$ which turns out to be 0 as the particle will definitely hit the absorbing wall at $x = 0$ given sufficient time. To get the approach to the stationary value $\mathcal{S}_\pm(x_0)$ for $\Delta < 0$ and the decay to 0 for $\Delta > 0$, at large t , we study the zeroes of $\mathcal{N}_-(0, s)$. Note from Eq. (63) that there is a simple pole at $s = 0$ which provides $\mathcal{S}_\pm(x_0)$ for $\Delta < 0$ and 0 for $\Delta > 0$. Subtracting this part we define $L_\pm(x_0, t) = S_\pm(x_0, t) - S_\pm(x_0, t \rightarrow \infty)$ which can be obtained from the poles of $\bar{S}_\pm(x_0, s)$ other than $s = 0$ on the negative s axis. these poles come from the solution $\mathcal{N}_-(0, s) = 0$. For large t , the solution of $\mathcal{N}_-(0, s) = 0$ with largest real part (say s^*) sets the time scale for decay of $L_\pm(x_0, t)$. We get,

$$L_\pm(x_0, t) = -e^{\frac{\Delta x_0^2}{2vl}} e^{s^* t} \frac{\mathcal{N}_\pm(x_0, s^*)}{s^* \mathcal{N}'_-(0, s^*)}, \quad (66)$$

where s^* is the largest root of $\mathcal{N}_-(0, s^*) = 0$. In Figure 14(b) and 14(c), we have verified our analytic results with the numerical simulation and we observe excellent match.

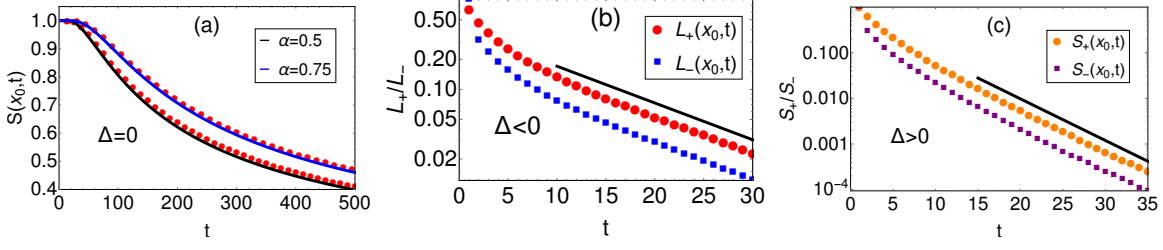


Figure 15. (a) Comparison of the analytic results of $S_{\pm}(x_0, t)$ in Eq. (72) with the numerical simulation for two different α and $\Delta = 0$. We have chosen $\gamma_1 = \gamma_2 = 1$, $v = 1$, $l = 1$ and $x_0 = 10$. (b) Simulation results of $L_{\pm}(x_0, t)$ for $\alpha = 0.5$ and $\Delta < 0$. We observe exponential decay of the form $e^{-\zeta t}$ with $\zeta = 0.085$. Parameters chosen for this plot are $\gamma_1 = 1.2$, $\gamma_2 = 1.5$, $v = 1$, $x_0 = 1$, and $l = 1$. (c) Simulation results for $S_{\pm}(x_0, t)$ for $\Delta > 0$. Here also we see exponential decay of the form $e^{-\zeta t}$ with $\zeta = 0.2097$. We have chosen $\gamma_1 = 2$, $\gamma_2 = 1$, $v = 1$, $x_0 = 1$, and $l = 1$.

3.3. General α

For this case it seems convenient to solve Eqs. (43) directly. Making analytical progress for arbitrary t seems difficult. We instead look at the large time limit which necessarily requires x_0 to be large so that the particle survives for long time. In this limit, the difference $H(x_0, t)$ of survival probabilities $U_{\pm}(x_0, t)$ of the particle starting with \pm velocities would decay fast (exponentially) which allows one to neglect the difference $H(x_0, t)$. Making the approximation, as we show in Appendix F, the equation for $\bar{U}(x_0, s)$ becomes,

$$s\bar{U}(x_0, s) = \frac{v^2 l^\alpha}{2\gamma} \partial_{x_0} \left(\frac{1}{x_0^\alpha} \partial_{x_0} \bar{U} \right) - \frac{v\Delta}{\gamma} \partial_{x_0} \bar{U}. \quad (67)$$

where $\bar{U}(x_0, s) = \bar{U}_+(x_0, s) + \bar{U}_-(x_0, s)$. To solve this equation, we need to specify the boundary conditions in terms of $\bar{U}(x_0, s)$. The boundary condition at $x_0 = 0$ discussed previously for $S_{\pm}(x_0, t)$ which can be translated in terms of $\bar{U}_{\pm}(x_0, s)$ as,

$$\bar{U}(0, s) = -\frac{2}{s}. \quad (68)$$

Note that we have neglected $\bar{H}(0, s)$ term in Eq. (68) as it decays faster than $\bar{U}(x_0, s)$. We now solve Eq. (67) separately for $\Delta = 0$ and $\Delta \neq 0$ cases.

3.3.1. $\Delta = 0$: For $\Delta = 0$, Eq. (67) reduces to

$$s\bar{U}(x_0, s) = D_\alpha \partial_{x_0} \left(\frac{1}{x_0^\alpha} \partial_{x_0} \bar{H} \right), \quad \text{with } D_\alpha = \frac{v^2 l^\alpha}{2\gamma} \quad (69)$$

This equation is solved in Appendix G and we here write the solution

$$\bar{U}(x_0, s) = -\frac{4x^{1+\alpha}}{\Gamma\left(\frac{1+\alpha}{2+\alpha}\right)} \frac{s^{-\frac{\alpha+3}{2(2+\alpha)}}}{((2+\alpha)\sqrt{D_\alpha})^{\frac{1+\alpha}{2+\alpha}}} K_{\frac{1+\alpha}{2+\alpha}}(2\sqrt{g_\alpha s}), \quad (70)$$

where $K_\nu(z)$ is the modified Bessel function of second kind and $g_\alpha = \frac{x^{2+\alpha}}{D_\alpha(2+\alpha)^2}$. To find the probability in time domain, one has to perform the inversion of the Laplace transforms. Looking at the expression of $\bar{U}(x_0, s)$, we use Eq. (25) to invert the Laplace transform.

$$\begin{aligned} S(x_0, t) &= \frac{S_+(x_0, t) + S_-(x_0, t)}{2}, \\ &= 1 - \frac{1}{2} L_{s \rightarrow t}^{-1} [\bar{U}(x_0, s)], \\ &= 1 - \frac{e^{-\frac{g_\alpha}{2t}}}{\Gamma\left(\frac{1+\alpha}{2+\alpha}\right)} \frac{x^{1+\alpha}}{\{(2+\alpha)\sqrt{D_\alpha}\}^{\frac{1+\alpha}{2+\alpha}} \sqrt{g_\alpha}} W_{-\frac{1}{2(2+\alpha)}, \frac{1+\alpha}{2(2+\alpha)}}\left(\frac{g_\alpha}{t}\right) \end{aligned} \quad (71)$$

To find asymptotics, we use the following representation of the Whittaker function $W_{m,k}(z) = e^{-\frac{z}{2}} z^{m+\frac{1}{2}} \mathcal{U}\left(\frac{1}{2} + m - k, 1 + 2m, z\right)$ in terms of the confluent hypergeometric function $\mathcal{U}(a, b, z)$ of second kind whose asymptotic behaviour as $z \rightarrow 0$ is $\mathcal{U}(a, b, z) \approx \frac{\Gamma(b-1)}{\Gamma(a)} z^{1-b} + \frac{\Gamma(1-b)}{\Gamma(a-b+1)}$ which gives,

$$S(x_0, t) = \frac{|\Gamma(-\frac{1+\alpha}{2+\alpha})|}{\Gamma\left(\frac{1+\alpha}{2+\alpha}\right) \Gamma\left(\frac{1}{2+\alpha}\right)} \frac{x_0^{1+\alpha}}{(2+\alpha)^{\frac{2(1+\alpha)}{2+\alpha}} (D_\alpha t)^{\frac{1+\alpha}{2+\alpha}}} \quad (72)$$

In Figure 15(a), we have plotted our analytic result in Eq. (71) and compared with the numerical simulation. We see excellent match between them for large x_0 . For small x_0 , our result in Eq. (71) does not match with simulation results as this expression is not valid although the power law decay $\left(1/t^{\frac{1+\alpha}{2+\alpha}}\right)$ is correctly predicted. This mismatch arises from the approximation $\bar{H}(x_0, s) \approx 0$ for large t , which is true only for large x_0 .

3.3.2. $\Delta < 0$: When $\Delta < 0$, the particle is drifted away from the origin with higher probability implying a non-zero survival probability for the particle even for infinite t . To find this probability we solve the original Eqs. (40) directly for the stationary value of the survival probability by putting $\partial_t S_\pm(x_0, t) = 0$. We present here the final expression of $S_\pm(x_0, t \rightarrow \infty)$ and relegate the details of derivation to Appendix H. Defining $\mathcal{S}_\pm(x_0) = S_\pm(x_0, t \rightarrow \infty)$, we get

$$\mathcal{S}_+(x_0) = 1 - \frac{\gamma - |\Delta|}{\gamma + |\Delta|} e^{-\frac{2|\Delta|}{v t^\alpha(\alpha+1)} x_0^{\alpha+1}}, \quad (73)$$

$$\mathcal{S}_-(x_0) = 1 - e^{-\frac{2|\Delta|}{v t^\alpha(\alpha+1)} x_0^{\alpha+1}}. \quad (74)$$

To study the approach to the steady state, we numerically find $S_\pm(x_0, t)$ and plot $L_\pm(x_0, t) = S_\pm(x_0, t) - \mathcal{S}_\pm(x_0)$ as functions of t in Figs. 15 (b). From these plots we see that the approach to the stationary values of both $S_\pm(x_0, t)$ is exponential with same relaxation time.

3.3.3. $\Delta > 0$: When $\Delta > 0$, the particle is drifted towards the origin. Unlike the previous case, the particle will now definitely hit the origin. In Figs. 15 (c), we numerically find that the survival probability decays exponentially to zero.

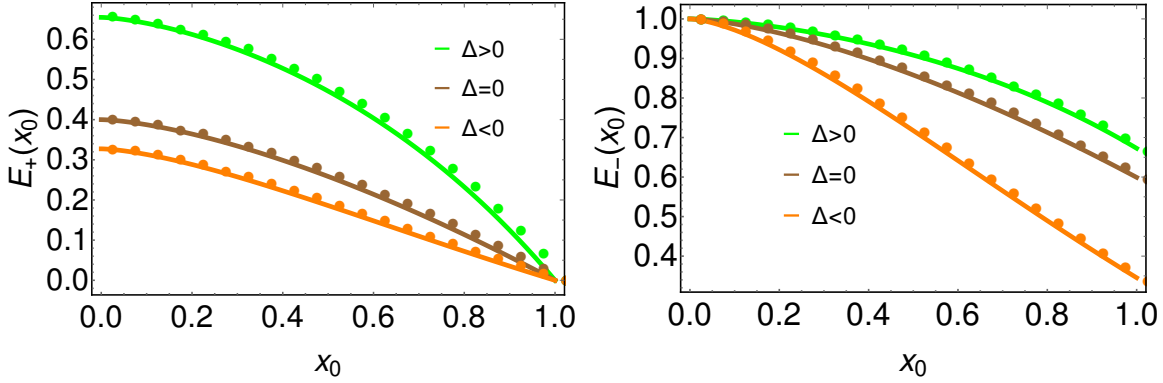


Figure 16. Comparison of the exit probability $E_{\pm}(x_0)$ given in Eqs. (77) and (78) with the numerical simulation of the same (filled circles) for $\alpha = 0.5$. The three curves correspond to (i) Green: $\gamma_1 = 2, \gamma_2 = 1$, (ii) Brown: $\gamma_1 = 1, \gamma_2 = 1$ and (iii) Orange: $\gamma_1 = 1, \gamma_2 = 2$. For both the figures, we have chosen $v = 1$ and $l = 1$

4. Exit probability of RTP from a finite interval for general α

In the previous sections, we have considered RTP in an infinite or semi-infinite line. This section deals with RTP in a finite interval $[0, M]$. The question that is addressed in this section is: what is the probability that the RTP will exit from the side $x = 0$ (or equivalently $x = M$) for general α . Let $E_{\pm}(x_0)$ denote the exit probability of the particle from side $x = 0$ starting from x_0 with velocity $\pm v$. Following [75], one can write a coupled backward equations for $E_{\pm}(x_0)$ and solve them explicitly. Below we discuss the derivation of these equations.

Consider that the RTP starts at x_0 with $+v$. In the small time dt , RTP can (i) flip its velocity with probability $R_1(x_0)\frac{dx}{v}$ and move to $x_0 - dx$ or (ii) continue to move with $+v$ velocity with probability $[1 - R_1(x_0)\frac{dx}{v}]$ and reach $x_0 + dx$. Starting from this new position, the particle then exits from $x = 0$ without touching $x = M$. One can then write for $E_{\pm}(x_0)$,

$$\begin{aligned} E_+(x_0) &= \left[1 - R_1(x_0)\frac{dx}{v}\right] E_+(x_0 + dx) + R_1(x_0)\frac{dx}{v} E_-(x_0 - dx), \\ E_-(x_0) &= \left[1 - R_2(x_0)\frac{dx}{v}\right] E_-(x_0 - dx) + R_2(x_0)\frac{dx}{v} E_+(x_0 + dx). \end{aligned} \quad (75)$$

Performing the Taylor's series expansion in dx and then taking $\Delta x \rightarrow 0$ limit, one gets the backward equations for $E_{\pm}(x_0)$ which read as,

$$\begin{aligned} v\partial_{x_0}E_+ - R_1(x_0)E_+ + R_1(x_0)E_- &= 0, \\ -v\partial_{x_0}E_- + R_2(x_0)E_+ - R_2(x_0)E_- &= 0. \end{aligned} \quad (76)$$

Note that the rates $R_1(x_0)$ and $R_2(x_0)$ are defined in Eq. (2). Before solving these equations, we need to specify the boundary conditions. The boundary conditions are $E_+(x_0 = M) = 0$ and $E_-(x_0 = 0) = 1$. The first boundary condition comes from the

fact that if the particle starts at $x_0 = M$ with positive velocity, it will exit from $x = M$ wall in the next time-step. Likewise the second boundary condition appears because if the particle starts from $x_0 = 0$ with $-v$, it will, in the next time-step exit from $x = 0$. Given these boundary conditions, one can solve these coupled differential equations in Eq. (76) for general α . After a straightforward but tedious calculation, we find the following final expressions for the exit probabilities

$$E_+(x_0) = \frac{e^{\bar{\Delta}M^{1+\alpha}} - e^{\bar{\Delta}x_0^{1+\alpha}}}{e^{\bar{\Delta}M^{1+\alpha}} - \frac{\gamma_2}{\gamma_1}}, \quad (77)$$

$$E_-(x_0) = \frac{e^{\bar{\Delta}M^{1+\alpha}} - \frac{\gamma_2}{\gamma_1} e^{\bar{\Delta}x_0^{1+\alpha}}}{e^{\bar{\Delta}M^{1+\alpha}} - \frac{\gamma_2}{\gamma_1}}, \quad (78)$$

where $\bar{\Delta} = \frac{2\Delta}{v(1+\alpha)t^\alpha}$. One can, in principle compute $E_\pm(x_0)$ also by integrating the current $j(0, t)$ through side $x = 0$ over all t . Although these two approaches yield the same result, the backward equation written in Eq. (76) is more illustrative and instructive specially for general α where the computation of $j(x, t)$ with absorbing barriers at $x = 0$ and $x = M$ is still a theoretical challenge. We also remark that taking $\Delta \rightarrow 0$ limit in Eqs. (77) and (78) correctly gives the results of [17] for $\alpha = 0$. In Figure (16), we have plotted our results in Eq. (77) and (78) with the numerical simulation of the same. The match between the two is excellent. In Figure (16), we notice that for a given x_0 , E_\pm is least for $\Delta < 0$ and largest for $\Delta > 0$. For $\Delta > 0$ ($\gamma_1 > \gamma_2$), the particle experiences an effective drift towards the origin which enhances the chance for particle to escape the origin. Similarly for $\Delta < 0$ ($\gamma_1 < \gamma_2$) the particle is drifted away from the origin.

Another interesting point to remark is that in the limit $M \rightarrow \infty$, $E_\pm(x_0)$ is equal to $1 - \mathcal{S}_\pm(x_0)$. One can easily verify that Eqs. (77) and (78) in this limit indeed reduce to 1 for $\Delta \geq 0$ and $1 - \mathcal{S}_\pm(x_0)$ for $\Delta < 0$ where $\mathcal{S}_\pm(x_0)$ is given by Eqs. (73) and (74) respectively.

5. Conclusions

To summarise, we have studied the motion of a run and tumble particle in one dimensional inhomogeneous media. The inhomogeneity was introduced by considering the position and direction dependent rates of flipping given in Eqs. (2). For $\gamma_1 > \gamma_2$, we have found that the particle reaches a stationary state in one dimension even in absence of any external confining potential. We have obtained an exact expression of the probability distribution given in Eq. (33), which characterises this non-equilibrium stationary state. The approach to this steady state is exponential for all $\alpha > 0$. While for $\alpha = 0$ and $\alpha = 1$ we have been able to compute the full distribution $P(x, t)$ which indeed shows exponential relaxation, for general $\alpha > 0$ performing exact calculation turned out to be difficult. We have provided heuristic argument for the exponential relaxation for general $\alpha > 0$ with strong numerical evidence.

	$\Delta > 0$	$\Delta = 0$	$\Delta < 0$
	Stationary state $P_\alpha^{st}(x)$ exists. See Eq. (33).	No stationary state, $P(x, t)$ with $\mu(t) = \langle x(t) \rangle = 0$	No stationary state, $P(x, t)$ with $\mu(t) \sim t$ $t \rightarrow \infty$
$\alpha = 0$	Relaxes as e^{-bt} to $P_0^{st}(x)$. See Eq. (19).	Exact expression for $P(x, t)$ given in Eq. (18) $\langle x^2(t) \rangle \sim t$ $t \rightarrow \infty$	Exact expression for $P(x, t)$ given in Eq. (18) $\sigma_0^2(t) \sim t$ $t \rightarrow \infty$
$\alpha = 1$	Relaxes as $e^{-\zeta t}$ to $P_1^{st}(x)$ with ζ given by the solution of Eq.(29)	Large t scaling form of $P(x, t)$ in Eq.(26). $\langle x^2(t) \rangle \sim t^{2/3}$. $t \rightarrow \infty$	$P(x, t)$ obtained from ILT of $\bar{P}(x, s)$ in Eq.(30), $\sigma_1^2(t) \sim \log(t)$
general $\alpha \geq 0$	Exponential relaxation verified numerically in Fig. 8b	Large t scaling form of $P(x, t)$ in Eq.(37), with $\langle x^2(t) \rangle \sim t^{\frac{2}{2+\alpha}}$. $t \rightarrow \infty$	Large t scaling form of , $P(x, t)$ in Eq. (39). for $\alpha \leq 1$, with $\sigma_\alpha^2(t) \simeq D_\alpha t^{1-\alpha}$.

Table 1. Table summarising $P(x, t)$ for various α and Δ . Here $\sigma_\alpha^2(t) = \langle x^2(t) \rangle - \langle |x(t)| \rangle^2$ and ILT stands for 'Inverse Laplace Transform'.

For $\gamma_1 \leq \gamma_2$ the RTP particle does not reach a stationary state. While for $\gamma_1 < \gamma_2$ the average absolute position $|x(t)|$ of the particle grows linearly with time, for $\gamma_1 = \gamma_2$, $\langle |x| \rangle = 0$. Note that the mean position $\langle x \rangle = 0$ in all cases. This suggests that the distribution $P(x, t)$ has two symmetric peaks moving with equal speed in the opposite direction for $\gamma_1 < \gamma_2$ and for $\gamma_1 = \gamma_2$ there is a single non-moving peak at $x = 0$. In this case for $\alpha = 0$ the distribution $P(x, t)$ was computed in [17] which was shown to be Gaussian at large t with variance growing linearly with time. In this paper we have extended this result for general $\alpha > 0$ for which we have found that $\langle x^2(t) \rangle \sim t^{\frac{2}{2+\alpha}}$. We also have proved that for large t , the distribution function $P(x, t)$ follows a scaling form $f_\alpha(y)$ with scaling variable $y = |x|/t^{1/(2+\alpha)}$ for $\gamma_1 = \gamma_2$. We have obtained an explicit expression of this scaling function for all $\alpha > 0$ in Eq. (37). On the other hand for $\gamma_1 < \gamma_2$, the distribution $P(x, t)$ does not satisfy this scaling form. In this case we have found that, the dynamics of the particle at large time can effectively be described by an Ito-Langevin equation with position dependent drift and diffusion constant (Note that such effective Ito-Langevin dynamics also holds for $\gamma_1 = \gamma_2$). While for $\alpha = 0$ and $\alpha = 1$, it is possible to solve the master equation exactly to find $P(x, t)$, performing the same task for general $\alpha > 0$ is difficult. In such cases the Ito-Langevin description is particularly useful to obtain the scaling behaviour of distribution $P(x, t)$ at large time

for $\gamma_1 < \gamma_2$ case (for which particle is drifted away from the origin). In particular, using this description we have shown that $\langle |x(t)| \rangle \sim t$ and $\sigma_\alpha^2(t) = \langle x^2(t) \rangle - \langle |x|(t) \rangle^2 \sim t^{1-\alpha}$ at large t for general α . In addition we have shown that scaling form of the distribution $P(x, t)$ is in fact Gaussian as also verified through direct numerical simulation of the actual RTP dynamics in Eq. (1).

We also have studied the survival probability of the inhomogenous RTP dynamics on semi-infinite line from an absorbing boundary at $x = 0$. For $\gamma_1 = \gamma_2$ the survival probability, at large t , decays as a power law with a persistent exponent θ *i.e.* $S(t) \sim t^{-\theta}$. We have shown that the persistent exponent is given by $\theta = \frac{1+\alpha}{2+\alpha}$ which generalises the result $\theta = 1/2$ for $\alpha = 0$ derived in [17]. For $\gamma_1 < \gamma_2$ the particle has non-zero probability to survive at $t \rightarrow \infty$ as it is effectively drifted away from the origin. We explicitly computed this non-zero survival probability for all $\alpha > 0$. On the other hand for $\gamma_1 > \gamma_2$, the probability decays to zero at large t . In both cases, we have found that the approach to the value at $t \rightarrow \infty$ is exponential. We have also looked at the exit probabilities of the RTP from a finite interval. Finally, we provide summary of the results presented in the paper in the tables 1 and 2.

	$\Delta > 0$	$\Delta = 0$	$\Delta < 0$
	$S(x_0, t) \xrightarrow{t \rightarrow \infty} 0$	$S(x_0, t) \xrightarrow{t \rightarrow \infty} 0$	$S(x_0, t) \xrightarrow{t \rightarrow \infty} \mathcal{S}(x_0)$ See Eqs. (73) and (74)
$\alpha = 0$	Exact expression of $S(x_0, t)$ given in Eq. (53). Decays to 0 exponentially.	Exact expression of $S(x_0, t)$ given in Eq.(53). Decays to 0 as $\sim \frac{1}{t^{1/2}}$ for large t .	Exact expression of $S(x_0, t)$ given in Eq.(53). Decays to $\mathcal{S}(x_0)$ exponentially.
$\alpha = 1$	Decays to zero as $e^{- s^* t}$ at large t , shown in Eq. (66)	Decays to zero as $\frac{1}{t^{2/3}}$ at large t , shown in Eqs. (61)	Relaxes to $\mathcal{S}_\pm(x_0)$ as $e^{- s^* t}$ at large t , shown in Eq. (66)
general $\alpha \geq 0$	For large t , decays to 0 exponentially. Verified numerically in Fig. 15c	For large t , decays to 0 as $t^{-\frac{1+\alpha}{2+\alpha}}$, see Eq.(72). Verified numerically in Fig. 15a	For large t , decays to $\mathcal{S}_\pm(x_0)$ exponentially. Verified numerically in Fig. 15b

Table 2. Table summarising $S_\pm(x_0, t)$ for various α and Δ .

We note that in this paper we have focused on the range $\alpha \geq 0$. However, we find that some of our results remain valid for $\alpha < 0$. For example the steady state distribution in case of $\gamma_1 > \gamma_2$, as given in Eq. (33) is also valid for $-1 < \alpha < 0$. In Fig. 8a we show a numerical verification of this fact for $\alpha = -0.3$. The scaling form $f_\alpha(y)$ of the probability distribution $P(x, t)$ for $\gamma_1 = \gamma_2$, given in Eq. (37). Quite remarkably it turns out that this scaling distribution holds true for $-2 < \alpha < 0$ also, which we have verified numerically (not shown here) as well. While these results remain

valid for $\alpha < 0$, many results, for example the scaling form of $P(x, t)$ given in Eq. (39) for $\gamma_1 < \gamma_2$ is not valid for $\alpha < 0$. Extending these results for $\alpha < 0$ remains an interesting future direction. All our results are valid in one dimension. Extending our results to higher dimension would be nice to explore. Recently it was shown that the survival probability for RTP in d -dimension has some universal features [44]. It would be interesting to see what happens to the universality when rates become position dependent. It would also be interesting to study the situation in which the rates R_1 , R_2 become time dependent where the time dependence may come from the coupling of the RTP motion to the evolution of the inhomogeneous media. Finally, to study more realistic situations where individual active agents like bacteria or micro-robots or Janus particle interacts among themselves, one needs to look at interacting particle dynamics which is another important future direction.

6. acknowledgement

The authors acknowledge fruitful discussions with Satya N Majumdar, Urna Basu and Varun Dubey. A.K would like to acknowledge support from the SERB Early Career Research Award ECR/2017/000634 from the Science and Engineering Research Board, Department of Science and Technology and the support of the Department of Atomic Energy, Government of India, under project no. 12-R&D-TFR-5.10-1100.

References

- [1] Ramaswamy S. 2010, The Mechanics and Statistics of Active Matter, *Annual Review of Condensed Matter Physics* **1** 323-345.
- [2] Romanczuk P., Bär M., Ebeling W., Lindner B. and Schimansky-Geier L. 2012, Active Brownian particles, *The European Physical Journal Special Topics* **202** 1-162.
- [3] Marchetti M. C., Joanny J. F., Ramaswamy S., Liverpool T. B., Prost J., Rao M. and Simha A. R. 2013, Hydrodynamics of soft active matter, *Rev. Mod. Phys.* **85** 1143.
- [4] Ramaswamy S. 2017, Active matter, *Journal of Statistical Mechanics: Theory and Experiment* **054002**.
- [5] Schweitzer F. 2003, Brownian Agents and Active Particles Collective Dynamics in the Natural and Social Sciences, *Springer, Berlin*.
- [6] Bechinger C., Di Leonardo R., Löwen H., Reichhardt C., Volpe G. and Volpe G. 2016, Active Particles in Complex and Crowded Environments, *Reviews of Modern Physics* **88** 045006.
- [7] Cates M. E. and Tailleur J. 2015, Motility-Induced Phase Separation, *Annual Review of Condensed Matter Physics* **6** 219-244.
- [8] Gonnella G., Marenduzzo D., Suma A. and Tiribocchi A. 2015, Motility-induced phase separation and coarsening in active matter, *Comptes Rendus Physique* **16** 316 - 331.
- [9] Partridge B. and Lee C. F. 2019, Critical Motility-Induced Phase Separation Belongs to the Ising Universality Class, *Phys. Rev. Lett.* **123** 068002.
- [10] Ballerini M., Cabibbo N., Candelier R., Cavagna A., Cisbani E., Giardina I., Lecomte V., Orlandi A., Parisi G., Procaccini A., Viale M. and Zdravkovic V. 2008, Interaction ruling animal collective behavior depends on topological rather than metric distance: Evidence from a field study, *Proc. Natl. Acad. Sci. USA* **105** 1232-37.
- [11] Katz Y., Tunström K., Ioannou C. C., Huepe C. and Couzin I. D. 2011, Inferring the structure and dynamics of interactions in schooling fish, *Proc. Natl. Acad. Sci. USA* **108** 18720-25.

- [12] Redner G. S., Hagan M. F. and Baskaran A. 2013, Structure and Dynamics of a Phase-Separating Active Colloidal Fluid, *Phys. Rev. Lett.* **110** 055701.
- [13] Bricard A., Caussin J. B., Desreumaux N., Dauchot O., and Bartolo D. 2013, Emergence of macroscopic directed motion in populations of motile colloids, *Nature* **503** 95.
- [14] Solon A. P., Fily Y., Baskaran A., Cates M., Kafri Y., Kardar M. and Tailleur J. 2015, Pressure is not a state function for generic active fluids, *Nature physics* **11** 673-678.
- [15] Li G. and Tang J. X. 2009, Accumulation of Microswimmers near a Surface Mediated by Collision and Rotational Brownian Motion, *Phys. Rev. Lett.* **103** 078101.
- [16] Elgeti J. and Gompper G. 2015 2015, Run-and-tumble dynamics of self-propelled particles in confinement, *Europhys. Lett.* **109** 58003.
- [17] Malakar K., Jemseena V., Kundu A., Kumar K. V., Sabhapandit S., Majumdar S. N., Redner S. and Dhar A. 2018, Steady state, relaxation and first- passage properties of a run-and-tumble particle in one-dimension *J. Stat. Mech.* 043215.
- [18] Erdmann U., Ebeling W. and Anishchenko V. S. 2002, Excitation of rotational modes in two-dimensional systems of driven Brownian particles., *Phys. Rev. E* **65** 061106.
- [19] Tailleur J. and Cates M. E. 2008, Statistical Mechanics of Interacting Run-and-Tumble Bacteria, *Phys. Rev. Lett.* **100** 218103.
- [20] Tailleur J. and Cates M. E. 2009, Sedimentation, trapping, and rectification of dilute bacteria, *Euro. Phys. Lett.* **86** 60002.
- [21] Das S., Gompper G. and Winkler R. G. 2018, Confined active Brownian particles: theoretical description of propulsion-induced accumulation, *New J. Phys.* **20** 015001.
- [22] Maggi C., Paoluzzi M., Pellicciotta N., Lepore L., Angelani L. and Leonardo R. D. 2014, Generalized Energy Equipartition in Harmonic Oscillators Driven by Active Baths, *Phys. Rev. Lett.* **113** 238303.
- [23] Maggi C., Marconi U., Gnan N. and Leonardo R. D. 2015, Multidimensional stationary probability distribution for interacting active particles, *Scientific Reports* **5**, 10742.
- [24] Erdmann U., Ebeling W. , Schimansky-Geier L. and Schweitzer F. 2000, Brownian particles far from equilibrium, *Eur. Phys. J. B* **15** 105.
- [25] Basu U., Majumdar S. N., Rosso A. and Schehr G. 2018, Active Brownian motion in two dimensions, *Phys. Rev. E* **98** 062121.
- [26] Malakar K., Das A., Kundu A., Kumar K. V. and Dhar A. 2020, Steady state of an active Brownian particle in a two-dimensional harmonic trap, *Phys. Rev. E* **101** 022610.
- [27] Pototsky A. and Stark H. 2012, Active Brownian particles in two-dimensional traps, *EPL* **98** 50004.
- [28] Basu U., Majumdar S. N., Rosso A. and Schehr G. 2019, Long-time position distribution of an active Brownian particle in two dimensions, *Phy. Rev. E* **100** 062116.
- [29] Solon A. P., Cates M. E. and Tailleur J. 2015, Active Brownian Particles and Run-and-Tumble Particles: a Comparative Study, *Eur. Phys. J. Spec. Top.* **224** 1231-1262.
- [30] Berg H. C. 2003, E. coli in Motion, *New York: Springer*.
- [31] Berg H. C. and Brown D. A. 1972, Chemotaxis in Escherichia coli analysed by three-dimensional tracking., *Nature* **239** 500-504.
- [32] Block S. M., Segall J. E. and Berg H. C. 1982, Impulse responses in bacterial chemotaxis., *Cell* **31** 215-226.
- [33] Behn U. and Schiele K. 1989, Stratonovich model driven by dichotomous noise: Mean first passage time, *Zeitschrift fr Physik B Condensed Matter volume* **77** 485-490.
- [34] Masoliver J. and Weiss G. H. 1993, On the maximum displacement of a one dimensional diffusion process described by the telegraphers noise, *Physica A* **195** 93-100.
- [35] Masoliver J. and Weiss G. H. 1996, Finite-velocity diffusion, *European Journal of Physics* **17** 190-196.
- [36] Weiss G. H. 2020, Some applications of persistent random walks and the telegrapher's equation, *Physica A: Statistical Mechanics and its Applications* **311** 381-410.
- [37] Bena I., Van den Broeck C., Kawai R. and Lindenberg K. 2002, Nonlinear response with

- dichotomous noise, *Phys. Rev. E* **66** 045603(R).
- [38] Weiss G. H. 1994, Aspects and applications of the random walk, *North-Holland, New York*.
- [39] Dhar A. and Chaudhuri D. 2002, Triple Minima in the Free Energy of Semiflexible Polymers, *Phys. Rev. Lett.* **89** 065502.
- [40] Masoliver J. and Lindenberg K. 2017, Continuous time persistent random walk: a review and some generalizations, *Eur. Phys. J. B* **90** 107.
- [41] Shee A., Dhar A. and Chaudhuri D. 2020, Active Brownian particles: mapping to equilibrium polymers and exact computation of moments, *preprint arXiv:2002.01815*.
- [42] Angelani L., Di Leonardo R. and Paoluzzi M. 2014, First-passage time of run-and-tumble particles, *Eur. Phys. J. E* **37** 59.
- [43] Scacchi A. and Sharma A. 2018, Mean first passage time of active Brownian particle in one dimension, *Molecular Physics* **116** 460-464.
- [44] Mori F., Doussal P. L., Majumdar S. N. and Schehr G. 2019, Universal survival probability for a d -dimensional run-and-tumble particle, *Preprint arXiv:2001.01492*.
- [45] Majumdar S. N. and Evans M. 2018, Run and tumble particle under resetting: a renewal approach, *Journal of Physics A: Mathematical and Theoretical* **51** 47.
- [46] Gradenigo G. and Majumdar S. N. 2019, A first-order dynamical transition in the displacement distribution of a driven run-and-tumble particle, *Journal of Statistical Mechanics: Theory and Experiment* 053206.
- [47] Banerjee T., Majumdar S. N., Rosso A. and Schehr G. 2019, Current fluctuations in non-interacting run-and-tumble particles in one-dimension, *Preprint arXiv:2001.01923*.
- [48] Santra I., Basu U. and Sabhapandit S. 2020, Position Distribution of Run-and-Tumble particles in Two-dimensions, *Preprint arXiv:2004.07562*.
- [49] Hartmann A. K., Majumdar S. N., Schawe H. and Schehr G. 2019, The convex hull of the run-and-tumble particle in a plane, *Preprint arXiv:1912.08778*.
- [50] Dhar A., Kundu A., Majumdar S. N., Sabhapandit S., and Schehr G. 2019, Run-and-tumble particle in one-dimensional confining potentials: Steady-state, relaxation, and first-passage properties, *Phys. Rev. E* **99** 032132.
- [51] Basu U., Majumdar S. N., Rosso A., Sabhapandit S. and Schehr G. 2020, Exact stationary state of a run-and-tumble particle with three internal states in a harmonic trap, *J. Phys. A: Math. Theor.* **53** 09LT01.
- [52] Doussal P. L., Majumdar S. N., Schehr G., 2020, Velocity and diffusion constant of an active particle in a one dimensional force field, *Preprint arXiv:2003.08155*.
- [53] Singh P. and Kundu A. 2019, Generalised 'Arcsine' laws for run-and-tumble particle in one dimension, *Journal of Statistical Mechanics: Theory and Experiment* 083205.
- [54] Slowman A. B., Evans M., and Blythe R. 2016, Jamming and Attraction of Interacting Run-and-Tumble Random Walkers, *Phys. Rev. Lett.* **116** 218101.
- [55] Slowman A. B., Evans M., and Blythe R. 2017, Exact Solution of Two Interacting Run-and-Tumble Random Walkers with Finite Tumble Duration, *Journal of Physics A: Mathematical and Theoretical* **50** 37.
- [56] Mallmin E., Blythe R. and Evans M. 2019, Exact spectral solution of two interacting run-and-tumble particles on a ring lattice, *J. Stat. Mech.* 013204.
- [57] Das A., Kundu A. and Dhar A. 2019, Gap statistics of two interacting run and tumble particles in one dimension, *preprint arXiv:1912.13269*.
- [58] Le Doussal P., Majumdar S. N. and Schehr G. 2019, Non-crossing run-and-tumble particles on a line, *Phys. Rev. E* **100** 012113.
- [59] Put S., Berx J. and Vanderzande C. 2019, Non-Gaussian anomalous dynamics in systems of interacting run-and-tumble particles, *Journal of Statistical Mechanics: Theory and Experiment* 123205.
- [60] Turner L., Ryu W. S. and Berg H. C. 2000, Real-time imaging of fluorescent flagellar filaments, *J Bacteriology* **182** 2793-2801.

- [61] de Gennes P. G. 2004, Chemotaxis: the role of internal delays, *European Biophysics Journal* **33** 691-693.
- [62] Adler J. 1973, A method for measuring chemotaxis and use of the method to determine optimum conditions for chemotaxis by *Escherichia coli*, *J. Gen. Microbiology* **74** 77-91.
- [63] Chatterjee S., Silveira R. and Kafri Y. 2011, Chemotaxis when Bacteria Remember: Drift versus Diffusion, *PLoS Comput. Biol.* **7** **12** e1002283.
- [64] Nava L. G., Großmann R. and Peruani F. 2018, Markovian robots: minimal navigation strategies for active particles, *Phys. Rev. E* **97** 042604.
- [65] Demaerel T. and Maes C. 2018, Active processes in one dimension, *Phys. Rev. E* **97** 032604.
- [66] Dev S. and Chatterjee S. 2019, Run-and-tumble motion with steplike responses to a stochastic input, *Phys. Rev. E* **99** 012402.
- [67] Rivero M. A., Tranquillo R. T., Buettner, Helen M. and Lauffenburger D. A. 1989, Transport models for chemotactic cell populations based on individual cell behavior, *Chemical Engineering Science* **44** 2881-2897.
- [68] Schnitzer M. J. 1993, Theory of continuum random walks and application to chemotaxis, *Phys. Rev. E* **48** 2553.
- [69] Farrell F. D.C., Marchetti C., Marenduzzo D. and Tailleur J. 2012, Pattern formation in self-propelled particles with density-dependent motility, *Physical review letters* **108** 248101.
- [70] Solon A., Stenhammar J., Cates M. E., Kafri Y. and Tailleur J. 2018, Generalized thermodynamics of phase equilibria in scalar active matter, *Phys. Rev. E* **97** 020602.
- [71] Angelani L. and Garra R., 2019, Run-and-tumble motion in one dimension with space-dependent speed, *Phys. Rev. E* **100** 052147.
- [72] Hentschel H. G. E. and Procaccia I. 1984, Relative diffusion in turbulent media: The fractal dimension of clouds, *Phys. Rev. A* **29** 1461.
- [73] Majumdar S. N. 1999, Persistence in Nonequilibrium Systems, *Current Science* **77** 370-375.
- [74] Randon-Furling J and Majumdar S. N. 2007, Distribution of the time at which the deviation of a Brownian motion is maximum before its first-passage time, *Journal of Statistical Mechanics: Theory and Experiment* **2007** P10008.
- [75] Redner S. 2001, A Guide to First-Passage Processes, *Cambridge University Press*.

Appendix A. Derivation of $G(x, s)$ and $\bar{P}(x, s)$ for $\alpha = 0$

In this appendix, we solve Eq. (15) explicitly to get $G(x, s)$. We will then insert this solution in Eqs. (10) and (13) to get $\bar{Q}(x, s)$ and $\bar{P}(x, s)$. Turning to Eq. (15), it is straightforward to solve it, and using the boundary conditions $G(x \rightarrow \pm\infty, s) = 0$, one gets

$$G(x, s) = \begin{cases} A_+ e^{-\lambda(s)x}, & \text{if } x > 0 \\ A_- e^{\lambda(s)x}, & \text{if } x < 0 \end{cases} \quad (\text{A.1})$$

where A_{\pm} are position independent constants. Inserting this solution in Eq. (13), we get $\bar{Q}(x, s)$ which can again be substituted in Eq. (10) to get $\bar{P}(x, s)$.

$$\bar{Q}(x, s) = \begin{cases} A_+ e^{-(\lambda(s) + \frac{\Delta}{v})x}, & \text{if } x > 0 \\ A_- e^{(\lambda(s) + \frac{\Delta}{v})x}, & \text{if } x < 0 \end{cases} \quad (\text{A.2})$$

$$\bar{P}(x, s) = \frac{v}{s} \left(\lambda(s) + \frac{\Delta}{v} \right) \begin{cases} A_+ e^{-(\lambda(s) + \frac{\Delta}{v})x}, & \text{if } x > 0 \\ -A_- e^{(\lambda(s) + \frac{\Delta}{v})x}, & \text{if } x < 0 \end{cases} \quad (\text{A.3})$$

The task now is to evaluate the constants A_{\pm} which demand two conditions. One condition comes by integrating Eq. (10) from $-\epsilon$ to $+\epsilon$ and take $\epsilon \rightarrow 0$. This will result in the following discontinuity equation

$$\bar{Q}(x \rightarrow 0^+, s) - \bar{Q}(x \rightarrow 0^-, s) = \frac{1}{v}. \quad (\text{A.4})$$

The other condition comes by noting that for symmetric initial condition, the probability distribution $P(x, t)$ is symmetric about $x = 0$ which gives

$$\bar{P}(x \rightarrow 0^+, s) = \bar{P}(x \rightarrow 0^-, s). \quad (\text{A.5})$$

Inserting the solutions of $Q(x, s)$ and $P(x, s)$ in Eqs. (A.4) and (A.5), we get two linear equations for A_+ and A_- solving which one finally gets complete expressions for $P(x, s)$ as,

$$\bar{P}(x, s) = \frac{1}{2s} \left(\lambda(s) + \frac{\Delta}{v} \right) e^{-(\lambda(s) + \frac{\Delta}{v})|x|}. \quad (\text{A.6})$$

This expression for $\bar{P}(x, s)$ is also written in Eq. (16).

Appendix B. Derivation of $P(x, t)$ for $\alpha = 0$ in Eq. (18)

In this appendix we will derive the expression for $P(x, t)$ for $\alpha = 0$ as written in Eq. (18). As we will see later, to prove this result the following inverse Laplace transform will be useful

$$L_{s \rightarrow t} [e^{-\lambda(s)y}] = -v \frac{d}{dy} \left[e^{-\gamma t} I_0 \left(\sqrt{\gamma_1 \gamma_2 \left(t^2 - \frac{y^2}{v^2} \right)} \right) \Theta(vt - y) \right], \quad (\text{B.1})$$

$$\text{where } \lambda(s) = \frac{1}{v} \sqrt{\Delta^2 + 2\gamma s + s^2}. \quad (\text{B.2})$$

So we first provide a derivation of this equation and then provide the derivation of Eq. (18).

Appendix B.1. Derivation of Eq. (B.1)

We begin with the following inversion.

$$L_{s \rightarrow t} \left[\frac{e^{-\lambda(s)y}}{\lambda(s)} \right] = \frac{1}{2\pi i} \int_{-i\infty}^{i\infty} ds e^{st} \frac{e^{-\lambda(s)y}}{\lambda(s)}. \quad (\text{B.3})$$

Proceeding further, we can rewrite $\lambda(s)$ as,

$$\lambda(s) = \frac{1}{v} \sqrt{(s + \gamma + \sqrt{\gamma_1 \gamma_2})(s + \gamma - \sqrt{\gamma_1 \gamma_2})}. \quad (\text{B.4})$$

Substituting this in Eq. (B.3), we get

$$L_{s \rightarrow t} \left[\frac{e^{-\lambda(s)y}}{\lambda(s)} \right] = \frac{v}{2\pi i} \int_{-i\infty}^{i\infty} ds e^{st} \frac{e^{-\frac{y}{v} \sqrt{(s+\gamma+\sqrt{\gamma_1\gamma_2})(s+\gamma-\sqrt{\gamma_1\gamma_2})}}}{\sqrt{(s+\gamma+\sqrt{\gamma_1\gamma_2})(s+\gamma-\sqrt{\gamma_1\gamma_2})}}. \quad (\text{B.5})$$

Changing the variable $s + \gamma - \sqrt{\gamma_1\gamma_2} = \sqrt{\gamma_1\gamma_2}z$ in Eq. (B.5), we have

$$\begin{aligned} L_{s \rightarrow t} \left[\frac{e^{-\lambda(s)y}}{\lambda(s)} \right] &= \frac{v}{2\pi i} e^{-(\gamma-\sqrt{\gamma_1\gamma_2})t} \int_{-i\infty}^{i\infty} dz e^{zt\sqrt{\gamma_1\gamma_2}} \frac{e^{-\frac{y\sqrt{\gamma_1\gamma_2}}{v} \sqrt{z(z+2)}}}{\sqrt{z(z+2)}}, \\ &= v e^{-(\gamma-\sqrt{\gamma_1\gamma_2})t} L_{z \rightarrow \sqrt{\gamma_1\gamma_2}t} \left[\frac{e^{-\frac{y\sqrt{\gamma_1\gamma_2}}{v} \sqrt{z(z+2)}}}{z(2+z)} \right]. \end{aligned} \quad (\text{B.6})$$

The inverse Laplace transform in the right hand side has been obtained in [58] (see Eq. (C2) there). Using this, we obtain,

$$L_{s \rightarrow t} \left[\frac{e^{-\lambda(s)y}}{\lambda(s)} \right] = v e^{-\gamma t} I_0 \left(\sqrt{\gamma_1\gamma_2} \left(t^2 - \frac{y^2}{v^2} \right) \right) \theta(vt - y), \quad (\text{B.7})$$

where I_0 is the modified Bessel function of first kind and $\theta(x)$ is the Heaviside step function. To prove (B.1), we note that

$$L_{s \rightarrow t} [e^{-\lambda(s)y}] = -\frac{d}{dy} \left[L_{s \rightarrow t} \left(\frac{e^{-\lambda(s)y}}{\lambda(s)} \right) \right]. \quad (\text{B.8})$$

Substituting Eq. (B.7) in (B.8), we establish the equality in (B.1).

Appendix B.2. Derivation of $P(x, t)$ in Eq. (16)

Let us begin by rewriting $\bar{P}(x, s)$ in Eq. (16) as,

$$\bar{P}(x, s) = -\frac{1}{2s} \frac{d}{d|x|} \left[e^{-(\lambda(s) + \frac{\Delta}{v})|x|} \right]. \quad (\text{B.9})$$

The inverse Laplace transform $P(x, t)$ read as,

$$\begin{aligned} P(x, t) &= -\frac{1}{2} \frac{d}{d|x|} \left[e^{-\frac{\Delta}{v}|x|} L_{s \rightarrow t} \left(\frac{e^{-\lambda(s)|x|}}{s} \right) \right], \\ &= -\frac{1}{2} \frac{d}{d|x|} \left[e^{-\frac{\Delta}{v}|x|} \int_0^t d\tau L_{s \rightarrow t-\tau} \left(\frac{1}{s} \right) L_{s \rightarrow \tau} (e^{-\lambda(s)|x|}) \right] \\ &= -\frac{1}{2} \frac{d}{d|x|} \left[e^{-\frac{\Delta}{v}|x|} \int_0^t d\tau L_{s \rightarrow \tau} (e^{-\lambda(s)|x|}) \right]. \end{aligned} \quad (\text{B.10})$$

In going from first line to second line, we have used the convolution property of Laplace transform. Inserting Eq. (B.1) in (B.10), one recovers the expression of $P(x, t)$ written in Eq. (18).

Appendix C. Derivation of the approximate expression of $P(x, t)$ given in Eq. (19) for $\alpha = 0$ at large t

Appendix C.1. $\Delta \geq 0$

Here we will provide a derivation of the large t behaviour of $P(x, t)$ for $\Delta > 0$ as written in Eq. (19). We begin with the exact expression of $P(x, t)$ in Eq. (18). We first rewrite Eq. (18) by replacing the time integral by $\int_0^t = \int_0^\infty - \int_t^\infty$ as

$$\begin{aligned} P(x, t) &= \frac{1}{2} e^{-\gamma_1 t} \delta(|x| - vt) + \frac{\gamma_1}{2v} \left(1 + \frac{\gamma_2 |x|}{2v} \right) e^{-\frac{\gamma_1 |x|}{2v}} \Theta(vt - |x|) \\ &\quad - \frac{\sqrt{\gamma_1 \gamma_2}}{2v} \int_0^\infty d\tau e^{-\gamma \tau} \frac{d \mathcal{I}(|x|, \tau)}{d|x|} \Theta(v\tau - |x|) \\ &\quad + \frac{\sqrt{\gamma_1 \gamma_2}}{2v} \int_t^\infty d\tau e^{-\gamma \tau} \frac{d \mathcal{I}(|x|, \tau)}{d|x|} \Theta(v\tau - |x|), \end{aligned} \quad (\text{C.1})$$

we note that as $t \rightarrow \infty$, $P(x, t)$ goes to the stationary distribution $P_0^{st}(x)$. Also at large t , the coefficient of δ -functions becomes very small. Hence for large t , we get

$$P(x, t) - P_0^{st}(x) \simeq \frac{\sqrt{\gamma_1 \gamma_2}}{2v} \int_t^\infty d\tau e^{-\gamma \tau} \frac{d \mathcal{I}(|x|, \tau)}{d|x|}. \quad (\text{C.2})$$

Note that $\mathcal{I}(x, t) = \frac{x e^{-\frac{\Delta x}{v}}}{v} \frac{I_1\left(\sqrt{\gamma_1 \gamma_2} \left(t^2 - \frac{x^2}{v^2}\right)\right)}{\sqrt{t^2 - \frac{x^2}{v^2}}}$ with I_1 being the modified Bessel function of first kind. One can easily perform the differentiation $\frac{d \mathcal{I}(|x|, \tau)}{d|x|}$ in Eq. (C.2). Also for large t , τ is also very large which means we can use the large τ form of $\frac{d \mathcal{I}(|x|, \tau)}{d|x|}$. It turns out that we need to make use of the asymptotic form of $I_\nu(z) \simeq \frac{e^z}{\sqrt{2\pi z}}$ for large z . For $vt \gg |x|$ alongwith the aforementioned approximations, we change the variable $\tau = tw$ to get

$$P(x, t) - P_0^{st}(x) \simeq \mathcal{C}_1 \int_1^\infty dw \frac{e^{-t\left(\mathcal{C}_2 w + \frac{\mathcal{C}_3}{w}\right)}}{w^{3/2}} \left(1 - \frac{\Delta|x|}{v} - \frac{x^2 \sqrt{\gamma_1 \gamma_2}}{v^2 t w} \right), \quad (\text{C.3})$$

where $\mathcal{C}_1 = \frac{(\gamma_1 \gamma_2)^{1/4}}{2v\sqrt{2\pi t}} e^{-\frac{\Delta|x|}{v}}$, $\mathcal{C}_2 = \gamma - \sqrt{\gamma_1 \gamma_2}$ and $\mathcal{C}_3 = \frac{x^2 \sqrt{\gamma_1 \gamma_2}}{2v^2 t^2}$. Interestingly this integration can be performed exactly. First we write,

$$\begin{aligned} \int_1^\infty dw \frac{e^{-t\left(\mathcal{C}_2 w + \frac{\mathcal{C}_3}{w}\right)}}{w^{3/2}} &= \int_0^\infty dw \frac{e^{-t\left(\mathcal{C}_2 w + \frac{\mathcal{C}_3}{w}\right)}}{w^{3/2}} - \int_0^1 dw \frac{e^{-t\left(\mathcal{C}_2 w + \frac{\mathcal{C}_3}{w}\right)}}{w^{3/2}}, \\ &= \sqrt{\frac{\pi}{\mathcal{C}_3 t}} e^{-2t\sqrt{\mathcal{C}_2 \mathcal{C}_3}} - Z_{3/2}, \end{aligned} \quad (\text{C.4})$$

$$(\text{C.5})$$

where Z_μ is defined as,

$$Z_\mu = \int_0^1 dw \frac{e^{-t\left(\mathcal{C}_2 w + \frac{\mathcal{C}_3}{w}\right)}}{w^\mu} \quad (\text{C.6})$$

Similarly,

$$\int_1^\infty dw \frac{e^{-t(\mathcal{C}_2 w + \frac{\mathcal{C}_3}{w})}}{w^{5/2}} = \frac{1}{2} \sqrt{\frac{\pi}{(\mathcal{C}_3 t)^3}} \left(1 + 2t\sqrt{\mathcal{C}_2 \mathcal{C}_3}\right) e^{-2t\sqrt{\mathcal{C}_2 \mathcal{C}_3}} - Z_{5/2}. \quad (\text{C.7})$$

Let us start by evaluating $Z_{1/2}$ which can be easily shown to be,

$$Z_{1/2} = \frac{1}{2} \sqrt{\frac{\pi}{\mathcal{C}_2 t}} e^{-2t\sqrt{\mathcal{C}_2 \mathcal{C}_3}} \left[1 + \text{Erf}\left(\sqrt{t\mathcal{C}_2} - \sqrt{t\mathcal{C}_3}\right) - e^{4t\sqrt{\mathcal{C}_2 \mathcal{C}_3}} \text{Erfc}\left(\sqrt{t\mathcal{C}_2} + \sqrt{t\mathcal{C}_3}\right)\right]. \quad (\text{C.8})$$

The integrals $Z_{3/2}$ and $Z_{5/2}$ can now be obtained from $Z_{3/2} = -\frac{d}{d\mathcal{C}_3} Z_{1/2}$ and $Z_{5/2} = -\frac{d}{d\mathcal{C}_3} Z_{3/2}$. We get

$$\begin{aligned} Z_{3/2} &= \frac{1}{2} \sqrt{\frac{\pi}{\mathcal{C}_3 t}} e^{-2t\sqrt{\mathcal{C}_2 \mathcal{C}_3}} \left[2 - \text{Erfc}\left(\sqrt{t\mathcal{C}_2} - \sqrt{t\mathcal{C}_3}\right) + e^{4t\sqrt{\mathcal{C}_2 \mathcal{C}_3}} \text{Erfc}\left(\sqrt{t\mathcal{C}_2} + \sqrt{t\mathcal{C}_3}\right)\right], \\ Z_{5/2} &= \frac{1}{2} \sqrt{\frac{\pi}{(\mathcal{C}_3 t)^3}} e^{-2t\sqrt{\mathcal{C}_2 \mathcal{C}_3}} \left[1 + 2t\sqrt{\mathcal{C}_2 \mathcal{C}_3} - \frac{1}{2} \left(1 + 2t\sqrt{\mathcal{C}_2 \mathcal{C}_3}\right) \text{Erfc}\left(\sqrt{t\mathcal{C}_2} - \sqrt{t\mathcal{C}_3}\right)\right. \\ &\quad \left. + \frac{1}{2} \left(1 - 2t\sqrt{\mathcal{C}_2 \mathcal{C}_3}\right) e^{4t\sqrt{\mathcal{C}_2 \mathcal{C}_3}} \text{Erfc}\left(\sqrt{t\mathcal{C}_2} + \sqrt{t\mathcal{C}_3}\right)\right] + \frac{1}{\mathcal{C}_3 t} e^{-t(\mathcal{C}_2 + \mathcal{C}_3)}. \end{aligned} \quad (\text{C.9})$$

Using these explicit expressions of $Z_{3/2}$ and $Z_{5/2}$, one gets explicit expression for the integrals in Eqs. (C.5) and (C.7). Finally, substituting these results in Eq. (C.3) we get the result written in Eq. (19) valid for large t . This technique can also be used to evaluate the asymptotic form for $\gamma_1 = \gamma_2$.

Appendix C.2. $\Delta < 0$

Here we will provide a derivation of the large t behaviour of $P(x, t)$ for $\Delta \leq 0$ case using saddle point approximation. Using the expression of $\bar{P}(x, s)$ in Eq. (16), we write $\bar{P}(x, t)$ as Bromwich integral as

$$P(x, t) = \frac{e^{-t\Delta\bar{x}}}{2\pi i} \int_{\gamma_0 - i\infty}^{\gamma_0 + i\infty} ds \left(\frac{\lambda(s) + \Delta}{2s}\right) e^{t\phi(s)}, \quad (\text{C.10})$$

where $\bar{x} = \frac{|x|}{vt}$, $\lambda(s) = \frac{1}{v} \sqrt{\Delta^2 + 2\gamma s + s^2}$ and $\phi(s)$ is given by

$$\phi(s) = s - \bar{x}v\lambda(s). \quad (\text{C.11})$$

From Eq. (C.10), we see that for $t \rightarrow \infty$ the integral will be dominated by the saddle point of $\phi(s)$. The saddle points are given by the solution of $\frac{d\phi}{ds} = 0$. It may look like that this equation has two solutions s_{\pm}

$$s_{\pm} = -\gamma \pm \sqrt{\frac{\gamma^2 - \Delta^2}{1 - \bar{x}^2}}, \quad (\text{C.12})$$

however only s_+ satisfies $\frac{d\phi}{ds} = 0$. Expanding $\phi(s)$ about s_+ and substituting in Eq. (C.10), we get

$$\begin{aligned}
P(x, t) &\simeq \frac{e^{t[\phi(s_+) - \Delta \bar{x}]}}{2\pi i} \left(\frac{\lambda(s_+) + \Delta}{2s_+} \right) \int_{\gamma_0 - i\infty}^{\gamma_0 + i\infty} ds e^{t \frac{\phi''(s_+)}{2} (s - s_+)^2}, \\
&\simeq \frac{e^{t[\phi(s_+) - \Delta \bar{x}]}}{2\pi} \left(\frac{\lambda(s_+) + \Delta}{2s_+} \right) \int_{-\infty + i(s_+ + \gamma_0)}^{\infty + i(s_+ + \gamma_0)} dy e^{-t \frac{\phi''(s_+)}{2} y^2} \\
&\simeq \frac{e^{t[\phi(s_+) - \Delta \bar{x}]}}{2\pi} \left(\frac{\lambda(s_+) + \Delta}{2s_+} \right) \int_{-\infty}^{\infty} dz e^{-t \frac{\phi''(s_+)}{2} z^2}, \tag{C.13}
\end{aligned}$$

In going from first to second line, we have changed the integration from complex domain to real line by substituting $s - s_+ = iy$ and from second to third line we have used the fact that $\phi''(s_+) = \frac{d\phi}{ds}|_{s_+} = \frac{(1-\bar{x})^{3/2}}{\bar{x}^2 \sqrt{\gamma^2 - \Delta^2}}$ is greater than zero. This also implies that the integral in Eq. (C.13) is always convergent. Performing the integration gives the asymptotic behaviour of $P(x, t)$ as written in Eq. (19).

Appendix D. Derivation of $G(x, s)$ and $\bar{P}(x, s)$ for $\alpha = 1$

In this appendix, we will provide the solution of $G(x, s)$ for $\alpha = 1$ as given in Eq. (20). We consider $\Delta = 0$ and $\Delta \neq 0$ cases separately.

Appendix D.1. Case I: $\Delta = 0$

We make the change of variable $x = \left(\frac{v^2 l}{2\gamma s} \right)^{\frac{1}{3}} y$ and then write Eq. (21) in terms of y as,

$$\partial_y^2 G - \left(|y| + d s^{\frac{4}{3}} \right) G = 0, \tag{D.1}$$

where $d = \left(\frac{2\gamma}{v^2 l} \right)^{\frac{1}{3}} \frac{l}{2\gamma}$. Solving this equation gives $G(y, s)$ in terms of Airy functions $\text{Ai} \left(|y| + d s^{\frac{4}{3}} \right)$ and $\text{Bi} \left(|y| + d s^{\frac{4}{3}} \right)$. However $\text{Bi}(y \rightarrow \infty)$ diverges while $G(y, s)$ should remain finite. We thus get

$$G(y, s) = \begin{cases} C_+ \text{Ai} \left(c s^{\frac{1}{3}} x + d s^{\frac{4}{3}} \right), & \text{if } x > 0 \\ C_- \text{Ai} \left(-c s^{\frac{1}{3}} x + d s^{\frac{4}{3}} \right), & \text{if } x < 0 \end{cases} \tag{D.2}$$

$$\bar{P}(y, s) = -\frac{1}{2s} \frac{d}{dx} \begin{cases} C_+ \text{Ai} \left(c s^{\frac{1}{3}} x + d s^{\frac{4}{3}} \right), & \text{if } x > 0 \\ -C_- \text{Ai} \left(-c s^{\frac{1}{3}} x + d s^{\frac{4}{3}} \right), & \text{if } x < 0 \end{cases} \tag{D.3}$$

Next we evaluate the constants C_+ and C_- . Before that, following Eq. (13) one sees that $\bar{Q}(x, s)$ and $G(x, s)$ are same for this case. We now integrate Eq. (10) from $-\epsilon$ to ϵ and take $\epsilon \rightarrow 0$ limit which gives discontinuity equation in $G(x, s)$. Also for symmetric

initial condition, the probability distribution will be symmetric about $x = 0$ which means $\bar{P}(x, s)$ is continuous about $x = 0$. Therefore, one finally gets

$$\begin{aligned} G(x \rightarrow 0^+, s) - G(x \rightarrow 0^-, s) &= \frac{1}{v}, \\ \bar{P}(x \rightarrow 0^+, s) &= \bar{P}(x \rightarrow 0^-, s), \end{aligned} \quad (\text{D.4})$$

These equations give rise to two linear equations for C_{\pm} which can be easily solved to get them as function of s . Next inserting $C_{\pm}(s)$ in Eqs.(D.2), one finally gets Eq. (22) for $\bar{P}(x, s)$.

Appendix D.2. Case II: $\Delta \neq 0$

At first, we make the transformation $\frac{z}{\sqrt{2}} = \frac{|\Delta|}{vl}x + \text{sgn}(x)\frac{\gamma s}{|\Delta|}\sqrt{\frac{l}{v|\Delta|}}$, which reduces Eq. (20) to

$$\partial_z^2 G - \left(\frac{z^2}{4} - \beta s^2 + \frac{\text{sgn}(\Delta)}{2} \right) G = 0 \quad (\text{D.5})$$

where $\beta = \frac{l(\gamma^2 - \Delta^2)}{2v|\Delta|^3}$. This equation is a standard one in the literature whose solution is given by parabolic cylinder functions $D_{\beta s^2 - \frac{1+\text{sgn}(\Delta)}{2}}(\pm z)$. Recalling $D_{\mu}(-|z|)$ diverges for some $\mu(s)$ as $z \rightarrow \pm\infty$, one gets the solution for $G(x, s)$ as

$$G(x, s) = \begin{cases} B_+ D_{\beta s^2 - \frac{1+\text{sgn}(\Delta)}{2}} \left(\sqrt{\frac{2|\Delta|}{vl}} \left(x + \frac{\gamma sl}{\Delta^2} \right) \right), & \text{if } x > 0 \\ B_- D_{\beta s^2 - \frac{1+\text{sgn}(\Delta)}{2}} \left(\sqrt{\frac{2|\Delta|}{vl}} \left(-x + \frac{\gamma sl}{\Delta^2} \right) \right), & \text{if } x < 0 \end{cases} \quad (\text{D.6})$$

where B_{\pm} are the position independent constants. Next we use Eq. (13) to write $\bar{Q}(x, s)$ and Eq. (10) to write $\bar{P}(x, s)$ as

$$\bar{Q}(x, s) = e^{-\frac{\Delta}{2vl}x^2} \begin{cases} B_+ D_{\beta s^2 - \frac{1+\text{sgn}(\Delta)}{2}} \left(\sqrt{\frac{2|\Delta|}{vl}} \left(x + \frac{\gamma sl}{\Delta^2} \right) \right), & \text{if } x > 0 \\ B_- D_{\beta s^2 - \frac{1+\text{sgn}(\Delta)}{2}} \left(\sqrt{\frac{2|\Delta|}{vl}} \left(-x + \frac{\gamma sl}{\Delta^2} \right) \right), & \text{if } x < 0 \end{cases} \quad (\text{D.7})$$

$$\bar{P}(x, s) = -\frac{1}{2s} \begin{cases} B_+ \frac{d}{dx} \left[e^{-\frac{\Delta}{2vl}x^2} D_{\beta s^2 - \frac{1+\text{sgn}(\Delta)}{2}} \left(\sqrt{\frac{2|\Delta|}{vl}} \left(x + \frac{\gamma sl}{\Delta^2} \right) \right) \right], & \text{if } x > 0 \\ -B_- \frac{d}{dx} \left[e^{-\frac{\Delta}{2vl}x^2} D_{\beta s^2 - \frac{1+\text{sgn}(\Delta)}{2}} \left(\sqrt{\frac{2|\Delta|}{vl}} \left(-x + \frac{\gamma sl}{\Delta^2} \right) \right) \right], & \text{if } x < 0 \end{cases} \quad (\text{D.8})$$

To evaluate constants B_{\pm} we need two conditions. The first one comes by integrating Eq. (10) from $-\epsilon$ to $+\epsilon$ and taking $\epsilon \rightarrow 0$ limit which gives discontinuity equation for $\bar{Q}(x, s)$. The other condition comes by noting that for symmetric initial condition, $\bar{P}(x, s)$ is symmetric about $x = 0$. These two conditions can be summarised as

$$\begin{aligned} \bar{Q}(x \rightarrow 0^+, s) - \bar{Q}(x \rightarrow 0^-, s) &= \frac{1}{v}, \\ \bar{P}(x \rightarrow 0^+, s) &= \bar{P}(x \rightarrow 0^-, s), \end{aligned} \quad (\text{D.9})$$

and they give rise to two linear equations for B_+ and B_- solving which we get B_{\pm} as function of s . Inserting the solution for $B_{\pm}(s)$ in Eq. (D.7), we get the final expression for $\bar{P}(x, s)$ which is written in Eq. (27)

Appendix E. Derivation of the asymptotic forms of $S_{\pm}(x_0, t)$ for $\alpha = 0$

Here we provide the derivation of $S_{\pm}(x_0, t)$ for large t for $\alpha = 0$ as given in Eqs. (55) and (56). Let us begin with the exact expression of $S_-(x_0, t)$ in Eq. (53). In this expression, writing $\int_0^t = \int_0^{\infty} - \int_t^{\infty}$, one gets

$$S_-(x_0, t) = 1 + ve^{\frac{\Delta x_0}{v}} \frac{d}{dx_0} \left[\int_0^{\infty} d\tau e^{-\gamma\tau} I_0 \left(\sqrt{\gamma_1 \gamma_2 \left(\tau^2 - \frac{x_0^2}{v^2} \right)} \right) \Theta(v\tau - x_0) \right] - ve^{\frac{\Delta x_0}{v}} \frac{d}{dx_0} \left[\int_t^{\infty} d\tau e^{-\gamma\tau} I_0 \left(\sqrt{\gamma_1 \gamma_2 \left(\tau^2 - \frac{x_0^2}{v^2} \right)} \right) \Theta(v\tau - x_0) \right]. \quad (\text{E.1})$$

Note that in the limit $t \rightarrow \infty$, the third term becomes zero. Hence we can rewrite Eq. (E.1) as,

$$S_-(x_0, t) = S_-(x_0, t \rightarrow \infty) - ve^{\frac{\Delta x_0}{v}} \frac{d}{dx_0} \left[\int_t^{\infty} d\tau e^{-\gamma\tau} I_0 \left(\sqrt{\gamma_1 \gamma_2 \left(\tau^2 - \frac{x_0^2}{v^2} \right)} \right) \Theta(v\tau - x_0) \right], \quad (\text{E.2})$$

where $S_-(x_0, t \rightarrow \infty)$ is 0 for $\Delta > 0$ and $\mathcal{S}_-(x_0)$ in Eq. (54) for $\Delta < 0$. The Heaviside step function inside integration becomes redundant when $vt > x_0$. Performing the differentiation over x_0 and changing the variable $\tau = ut$, we get

$$L_-(x_0, t) = \frac{x_0}{v} \sqrt{\gamma_1 \gamma_2} e^{\frac{\Delta x_0}{v}} \int_1^{\infty} du \frac{e^{-\gamma ut}}{\sqrt{u^2 - \frac{x_0^2}{v^2 t^2}}} I_1 \left(\sqrt{\gamma_1 \gamma_2 \left(u^2 t^2 - \frac{x_0^2}{v^2} \right)} \right), \quad (\text{E.3})$$

where $L_-(x_0, t) = S_-(x_0, t) - S_-(x_0, t \rightarrow \infty)$. Note that in the integration, u is greater than or equal to 1. Hence for large t , we can use the asymptotic form of modified Bessel functions $I_{\nu}(z) \simeq \frac{e^z}{\sqrt{2\pi z}}$ for large z . Therefore for large t , we have

$$L_-(x_0, t) \simeq e^{\frac{\Delta x_0}{v}} \frac{x_0}{v} \frac{(\gamma_1 \gamma_2)^{\frac{1}{4}}}{\sqrt{2\pi t}} \int_1^{\infty} \frac{du}{u^{3/2}} e^{-ut(\gamma - \sqrt{\gamma_1 \gamma_2})}. \quad (\text{E.4})$$

This integration can be now easily performed as,

$$\begin{aligned} \int_1^{\infty} \frac{du}{u^{3/2}} e^{-uty} &= 2e^{-yt} - 2\sqrt{\pi yt} \operatorname{Erfc}[\sqrt{yt}], \\ &\simeq \frac{e^{-yt}}{yt}. \end{aligned} \quad (\text{E.5})$$

In going from first line to second line we have used that for large t , $\operatorname{Erfc}[\sqrt{yt}] \simeq e^{-yt} \left(\frac{1}{\sqrt{\pi yt}} - \frac{1}{2\sqrt{\pi y^3 t^3}} \right)$. Substituting Eq. (E.5) in (E.4), one recovers the expressions in

Eq. (56). Proceeding similarly for $S_+(x_0, t)$ one gets Eq. (55) for large t from Eq. (53). It is worth remarkin that the analysis so far assumed that $\gamma_1 \neq \gamma_2$. However for $\gamma_1 = \gamma_2$ also, the same technique gives the correct asymptotic form as obtained in [17, 58] and written in Eqs. (55) and (56).

Appendix F. Effective equation for survival probability for general α at large t and large x_0

In this appendix, we will derive effective differential equations for $\bar{U}(x_0, s)$ which is related to $\bar{S}_\pm(x_0, s)$ using Eqs. (42) and (44). We start with Eqs.(43) for $\bar{U}_\pm(x_0, s)$

$$\begin{aligned} [-v\partial_{x_0} + R_1(x_0) + s] \bar{U}_+ &= R_1(x_0) \bar{U}_-, \\ [v\partial_{x_0} + R_2(x_0) + s] \bar{U}_- &= R_2(x_0) \bar{U}_+, \end{aligned} \quad (\text{F.1})$$

where $R_1(x_0)$ and $R_2(x_0)$ are defined in Eqs.(2). One may rewrite them as,

$$\frac{1}{x^\alpha} \mathcal{O}_+ \bar{U}_+ = \gamma_1 \bar{U}_-, \quad \text{with } \mathcal{O}_+ = -v\partial_x + \gamma_1 \frac{x^\alpha}{l^\alpha} + s, \quad (\text{F.2})$$

$$\frac{1}{x^\alpha} \mathcal{O}_- \bar{U}_- = \gamma_2 \bar{U}_+, \quad \text{with } \mathcal{O}_- = v\partial_x + \gamma_2 \frac{x^\alpha}{l^\alpha} + s. \quad (\text{F.3})$$

Operating both sides of Eq. (F.2) by \mathcal{O}_- and Eq. (F.3) by \mathcal{O}_+ , we can decouple these two equations and simplify them further to get

$$-v^2 l^\alpha \partial_{x_0} (x_0^{-\alpha} \partial_{x_0} \bar{U}_+) + v(\gamma_1 - \gamma_2) \partial_{x_0} \bar{U}_+ - \left[-\frac{vs\alpha l^\alpha}{x_0^{\alpha+1}} + \frac{s^2 l^\alpha}{x_0^\alpha} + (\gamma_1 + \gamma_2)s \right] \bar{U}_+ = 0, \quad (\text{F.4})$$

$$-v^2 l^\alpha \partial_{x_0} (x_0^{-\alpha} \partial_{x_0} \bar{U}_-) + v(\gamma_1 - \gamma_2) \partial_{x_0} \bar{U}_- - \left[\frac{vs\alpha l^\alpha}{x_0^{\alpha+1}} + \frac{s^2 l^\alpha}{x_0^\alpha} + (\gamma_1 + \gamma_2)s \right] \bar{U}_- = 0. \quad (\text{F.5})$$

Adding these two equations and recalling the definition in Eqs.(44), one gets

$$-v^2 l^\alpha \partial_{x_0} \left(\frac{1}{x_0^\alpha} \partial_{x_0} \bar{U} \right) + 2v\Delta \partial_{x_0} \bar{U} + \left(2\gamma s + \frac{s^2 l^\alpha}{x_0^\alpha} \right) \bar{U} - \frac{\alpha v s l^\alpha}{x_0^{\alpha+1}} \bar{H} = 0 \quad (\text{F.6})$$

For large t (equivalantly small s) behaviour, we neglect the $O(s^2)$ term. Also for large x_0 , we neglect the term containing H because this is sub leading with respect to $x_0^{-\alpha} \partial_{x_0} \bar{U}$, which itself is of order \bar{H} (see Eqs. (45) and (46)). The final equation thus reduces to Eq. (67) of the main text.

Appendix G. Solution of Effective equation for survival probability for general α and $\Delta = 0$

Here we provide solution of Eq. (69) for general α . Changing variable $y = x_0^{\frac{2+\alpha}{2}}$ and writing Eq. (69) in terms of y , we get

$$y \partial_y^2 \bar{U} - \frac{\alpha}{2+\alpha} \partial_y \bar{U} = \frac{4sy}{D_\alpha (2+\alpha)^2} \bar{U}. \quad (\text{G.1})$$

The solutions of this equation are given in terms of modified Bessel functions of first kind and second kind $y^{\frac{1+\alpha}{2+\alpha}} I_{\frac{1+\alpha}{2+\alpha}} \left(\frac{2}{2+\alpha} \sqrt{\frac{s}{D_\alpha}} y \right)$ and $y^{\frac{1+\alpha}{2+\alpha}} K_{\frac{1+\alpha}{2+\alpha}} \left(\frac{2}{2+\alpha} \sqrt{\frac{s}{D_\alpha}} y \right)$. However the first solution diverges as $x \rightarrow \infty$ which leaves us with only the second solution. Writing the solution in terms of x_0 , we get

$$\bar{U}(x_0, s) = B x_0^{\frac{1+\alpha}{2}} K_{\frac{1+\alpha}{2+\alpha}} \left(\frac{2}{2+\alpha} \sqrt{\frac{s}{D_\alpha}} x_0^{\frac{2+\alpha}{2}} \right). \quad (\text{G.2})$$

To get $\bar{H}(x_0, s)$ we add the Eqs.(F.1) which gives

$$\bar{H}(x_0, s) = v \left(s + \frac{2\gamma x_0^\alpha}{l^\alpha} \right) \partial_{x_0} U. \quad (\text{G.3})$$

To evaluate the constant B , we use the other boundary condition $S_-(0, s) = \frac{1}{s} + \bar{U}_-(0, s) = 0$ which gives $\bar{U}_-(0, s) = -\frac{1}{s}$. Next to translate this in terms of $\bar{U}(x_0, s)$, we note that $\bar{U}_-(x_0, s) = \frac{\bar{U}(x_0, s) - \bar{H}(x_0, s)}{2}$ which gives the boundary condition in terms of $\bar{U}(x_0, s)$ and $\bar{H}(x_0, s)$ as,

$$U(0, s) - H(0, s) = -\frac{2}{s}. \quad (\text{G.4})$$

To find $U(0, s)$ and $H(0, s)$, we substitute $K_\nu(z) \approx 2^{\nu-1} z^{-\nu} \Gamma(\nu)$ as $z \rightarrow 0$ in Eqs.(G.2) and (G.3) which gives $H(0, s) = 0$ and non-zero $U(0, s)$. Finally substituting this in Eq. (G.4) gives $B(s)$ and the expression for $\bar{U}(x_0, s)$ which is written in Eq. (70)

Appendix H. $S_\pm(x_0, t)$ as $t \rightarrow \infty$ for general α and $\Delta < 0$

In this appendix, we will solve Eqs. (40) for general α and $\Delta < 0$ in the limit $t \rightarrow \infty$. For $\Delta < 0$, the particle is effectively drifted away from the absorbing wall at origin which gives rise to non-zero S_\pm as $t \rightarrow \infty$. For this case Eqs.(40) can be rewritten as,

$$\left(-v \frac{d}{dx_0} + \frac{\gamma_1 x_0^\alpha}{l^\alpha} \right) S_+ = \frac{\gamma_1 x_0^\alpha}{l^\alpha} S_-, \quad (\text{H.1})$$

$$\left(v \frac{d}{dx_0} + \frac{\gamma_2 x_0^\alpha}{l^\alpha} \right) S_- = \frac{\gamma_2 x_0^\alpha}{l^\alpha} S_+. \quad (\text{H.2})$$

These two equations can be recasted as,

$$\frac{l^\alpha}{x_0^\alpha} \mathcal{L}_+ S_+ = \gamma_1 S_-, \quad \text{with } \mathcal{L}_+ = -v \frac{d}{dx_0} + \frac{\gamma_1 x_0^\alpha}{l^\alpha} \quad (\text{H.3})$$

$$\frac{l^\alpha}{x_0^\alpha} \mathcal{L}_- S_- = \gamma_2 S_+, \quad \text{with } \mathcal{L}_- = v \frac{d}{dx_0} + \frac{\gamma_2 x_0^\alpha}{l^\alpha}. \quad (\text{H.4})$$

These coupled equations can be easily decoupled by multiplying both sides of Eq(H.3) by \mathcal{L}_- which gives ordinary differential equation for $S_+(x_0)$ as,

$$\frac{d}{dx_0} \left(\frac{v l^\alpha}{x_0^\alpha} \frac{d}{dx_0} - 2\Delta \right) S_+ = 0. \quad (\text{H.5})$$

One can now solve Eq.(H.5) to get $S_+(x_0)$ which could be substituted in Eq.(H.1) to get $S_-(x_0)$. The solved expressions for $S_{\pm}(x_0)$ read as,

$$S_+(x_0) = C_1 + C_2 e^{-\frac{2|\Delta|}{vI\alpha(\alpha+1)}x_0^{\alpha+1}}, \quad (\text{H.6})$$

$$S_-(x_0) = C_1 + C_2 \frac{\gamma + |\Delta|}{\gamma - |\Delta|} e^{-\frac{2|\Delta|}{vI\alpha(\alpha+1)}x_0^{\alpha+1}}, \quad (\text{H.7})$$

where C_1 and C_2 are constants that remain to be evaluated. To evaluate them, we use the boundary conditions $S_{\pm}(x_0 \rightarrow \infty) = 0$ and $S_-(x_0 \rightarrow 0) = 0$ which give $C_1 = 1$ and $C_2 = -\frac{\gamma - |\Delta|}{\gamma + |\Delta|}$. Inserting them in Eqs. (H.6) and (H.7), one gets the final expression for $S_{\pm}(x_0)$ written in Eqs.(73) and (74).